BEST AVAILABLE IMAGES

Defective images within this document are accurate representations of the original documents submitted by the applicant.

Defects in the images may include (but are not limited to):

- BLACK BORDERS
- TEXT CUT OFF AT TOP, BOTTOM OR SIDES
- FADED TEXT
- ILLEGIBLE TEXT
- SKEWED/SLANTED IMAGES
- COLORED PHOTOS
- BLACK OR VERY BLACK AND WHITE DARK PHOTOS
- GRAY SCALE DOCUMENTS

IMAGES ARE BEST AVAILABLE COPY.

As rescanning documents *will not* correct images, please do not report the images to the Image Problem Mailbox.

THE JOURNAL OF BIOLOGICAL CHEMISTRY
Vol. 276, No. 5, Issue of February 2, pp. 3361–3370, 2001
Printed in U.S.A.

Hyaluronidase Induction of a WW Domain-containing Oxidoreductase That Enhances Tumor Necrosis Factor Cytotoxicity*

EXHIBIT A

Received for publication, August 7, 2000, and in revised form, October 25, 2000
Published, JBC Papers in Press, October 31, 2000, DOI 10.1074/jbc.M007140200

Nan-Shan Chang‡, Nicole Pratt, John Heath, Lori Schultz, Daniel Sleve, Gregory B. Carey, and Nicole Zevotek

From the Laboratory of Molecular Immunology, Guthrie Research Institute, Sayre, Pennsylvania 18840

To determine how hyaluronidase increases certain cancer cell sensitivity to tumor necrosis factor (TNF) cytotoxicity, we report here the isolation and characterization of a hyaluronidase-induced murine WW domain-containing oxidoreductase (WOX1). WOX1 is composed of two N-terminal WW domains, a nuclear localization sequence, and a C-terminal alcohol dehydrogenase (ADH) domain. WOX1 is mainly located in the mitochondria, and the mitochondrial targeting sequence was mapped within the ADH domain. Induction of mitochondrial permeability transition by TNF, staurosporine, and atractyloside resulted in WOX1 release from mitochondria and subsequent nuclear translocation. TNF-mediated WOX1 nuclear translocation occurred shortly after that of nuclear factor-κB nuclear translocation, whereas both were independent events. WOX1 enhanced TNF cytotoxicity in L929 cells via its WW and ADH domains as determined using stable cell transfectants. In parallel with this observation, WOX1 also enhanced TRADD (TNF receptor-associated death domain protein)-mediated cell death in transient expression experiments. Antisense expression of WOX1 raised TNF resistance in L929 cells. Enhancement of TNF cytotoxicity by WOX1 is due, in part, to its significant down-regulation of the apoptosis inhibitors Bcl-2 and Bcl-x_L (>85%), but up-regulation of pro-apoptotic p53 (~200%) by the ADH domain. When overexpressed, the ADH domain mediated apoptosis, probably due to modulation of expression of these proteins. The WW domains failed to modulate the expression of these proteins, but sensitized COS-7 cells to TNF killing and mediated apoptosis in various cancer cells independently of caspases. Transient cotransfection of cells with both p53 and WOX1 induced apoptosis in a synergistic manner. WOX1 colocalizes with p53 in the cytosol and binds to the proline-rich region of p53 via its WW domains. Blocking of WOX1 expression by antisense mRNA abolished p53 apoptosis. Thus, WOX1 is a mitochondrial apoptogenic protein and an essential partner of p53 in cell death.

Most cancer cells are known to secrete the matrix-degrading enzyme hyaluronidase. Elevation of hyaluronidase levels is associated with progression, invasion, and metastasis of breast, ovarian, endometrial, prostate, and other cancers (1–5). Also, expression of hyaluronidase by tumor cells induces angiogenesis *in vivo* (6). The growth of murine lung carcinoma and melanoma, for example, is influenced by *Hyal-1*, a locus determining hyaluronidase levels and polymorphism (7). How hyaluronidase modulates cell growth is not known.

Both *in vitro* and *in vivo* studies have shown that exogenous hyaluronidase reverses the resistance to chemotherapeutic drugs in cancer cells and solid tumors by increasing their exposure to the drugs (8–10). We have determined that hyaluronidase enhances cancer cell susceptibility to tumor necrosis factor (TNF)[1]-mediated cell death (11–13). For example, pretreatment of murine L929 fibroblasts and human prostate LNCaP cells with hyaluronidase for at least 12 h significantly increases their sensitivity to TNF-mediated death (100–700%) (11–13). The hyaluronidase-enhanced TNF sensitivity in L929 cells is associated, in part, with up-regulation of pro-apoptotic p53 (11–13).

To further explore the mechanism whereby hyaluronidase enhances TNF cytotoxicity, we report here the isolation of a novel murine WW domain-containing oxidoreductase (*Wox1*) cDNA. Hyaluronidase increased *Wox1* gene and protein expression. Ectopic expression of WOX1 in L929 cells enhanced their sensitivity to TNF cytotoxicity, whereas antisense *Wox1* raised TNF resistance. Thus, WOX1 is involved in the hyaluronidase-increased TNF sensitivity in various cancer cells. We produced polyclonal antibodies against WOX1, examined WOX1 cellular localization, and determined the possibility of WOX1 nuclear translocation in response to apoptotic stimuli and inducers of mitochondrial permeability transition. Overexpression of WOX1 was shown to induce cell death. We then examined whether the cell death was p53- or caspase-dependent. Since hyaluronidase up-regulates p53 expression, the role of p53 and WOX1 in mediating cell death was determined.

EXPERIMENTAL PROCEDURES

Molecular Cloning of Wox1—Isolation of novel cDNAs by differential display, library screening, and functional analysis has been described previously (14, 15). L929 cells were treated with bovine testicular hyaluronidase (200 units/ml; Sigma) for 4 h, followed by isolating total cellular RNA and performing first strand cDNA synthesis and differ-

* This work was supported by the Guthrie Foundation for Education and Research, the Wendy Will Case Cancer Fund, the American Heart Association, and National Cancer Institute Grants R01CA61879 and R55CA64423 from the National Institutes of Health (to N.-S. C.). The costs of publication of this article were defrayed in part by the payment of page charges. This article must therefore be hereby marked "*advertisement*" in accordance with 18 U.S.C. Section 1734 solely to indicate this fact.

The nucleotide sequence(s) reported in this paper has been submitted to the GenBank™/EBI Data Bank with accession number(s) AF187014 (murine Wox1) and AI669330 and AF187015 (human WOX3).

‡ To whom correspondence should be addressed: Lab. of Molecular Immunology, Guthrie Research Inst., 1 Guthrie Square, Sayre, PA 18840. Tel.: 570-882-4620; Fax: 570-882-4643; E-mail: nschang@inet.guthrie.org.

[1] The abbreviations used are: TNF, tumor necrosis factor; WOX1, WW domain-containing oxidoreductase-1; GFP, green fluorescent protein; ADH, alcohol dehydrogenase; NLS, nuclear localization sequence; SAPK/JNK, stress-activated protein kinase/c-Jun N-terminal kinase; NF, nuclear factor; COX4, cytochrome *c* oxidase subunit 4; TRADD, TNF receptor-associated death domain protein; AIF, apoptosis-inducing factor.

ential display (14, 15). A hyaluronidase-induced cDNA of 300 base pairs was isolated and used to screen a λ-phage cDNA library from murine NIH/3T3 fibroblasts (CLONTECH, Palo Alto, CA). The isolated full-length cDNA insert was amplified by polymerase chain reaction (using λ-phage primers) (see Table I) and subcloned into the TA cloning site of eukaryotic expression vector pCR3.1 (Invitrogen, San Diego, CA). Protein domain analysis was performed using the SMART Simple Modular Architecture Research Tool (16, 17). As compared with the existing domains in the universal data bases, each resulting positive domain is determined according to a calculated *E*-value (16, 17).

In Vitro Translation—The full-length murine *Wox1* cDNA was constructed in the pCR3.1 vector. An *in vitro* translation kit (Novagen, Madison, WI) was used to transcribe the full-length *Wox1*-pCR3.1 construct into mRNA via the T7 promoter and to translate into [^{35}S]methionine-labeled WOX1 protein.

Expression Constructs—Constructs, which were made with the pEGFP-C1 vector (CLONTECH), for expressing N-terminal green fluorescent protein (GFP)-tagged proteins are shown in Table I. These constructs were used to express the full-length coding region (construct 2), the antisense *Wox1* mRNA (expressing antisense *Wox1* mRNA and GFP protein; construct 3), the N-terminal WW domain region (construct 4), a partial ADH domain (amino acids 180–392; construct 5), and the potential mitochondrial targeting regions in the ADH domain (amino acids 180–273 and 209–273; constructs 6 and 7, respectively). To examine whether the large-size GFP protein (28 kDa) affects the WOX1 function, similar constructs, which were made with a small C-terminal v5 tag (5 kDa) in the pcDNA3.1.TOPO vector (Invitrogen), were used to express full-length WOX1 (construct 8), the first WW domain (construct 9), and the first and second WW domains (construct 10).

p53 Expression Construct—A full-length p53 cDNA clone from normal human tissues was found in the expressed sequence tag data base (GenBank™/EBI accession numbers AI243172 and AF307851) and obtained from Incyte Genomics (St. Louis, MO). The coding region was cloned into the pcDNA3.1/CTGFP-TOPO vector (Invitrogen) and tagged with a GFP sequence at the C terminus (construct 11) (see Table I).

Site-directed Mutagenesis—Site-directed mutagenesis was performed to alter several indicated sites in the *Wox1* cDNA sequence using the QuikChange site-directed mutagenesis Kit (Stratagene, La Jolla, CA). The aspartic acid residues of a putative caspase recognition site (DIND, amino acids 267–270) were mutated to glycine, *i.e.* D267G and D270G (construct 17) (see Table I). The GKRKRV sequence (amino acids 50–55) of the nuclear localization sequence (NLS) was also mutated to GQGTGV (construct 18) (see Table I).

Antibody Production—A WOX1 peptide (RLAFTVDDNPTKPTTRQRY, amino acids 89–107) was synthesized by Genemed Biotechnologies, Inc. (San Francisco, CA) and conjugated with keyhole limpet hemocyanin for antibody production in rabbits using the Pierce antibody production kit. The selected WOX1 sequence is identical between human and mouse.

Transient Transfection—In most cases, transfection studies were performed by our standard $CaPO_4$ precipitation method (14, 15). Forty-eight h post-transfection, the extent of cell death was measured by crystal violet staining (a measure of both necrosis and apoptosis). Additionally, DNA fragmentation assays (11) were performed to determine the extent of apoptosis. To exclude the possibility of nonspecific killing of cells caused by transfection reagents or vectors alone, the observed results were repeated using liposome-based cell transfection reagents such as LipofectAMINE (Amersham Pharmacia Biotech), GeneFECTOR (Venn Nova, Pompano Beach, FL), and FuGENE 6 (Roche Molecular Biochemicals) and electroporation (BTX ECM830, Genetronics, San Diego, CA).

Stable Transfectants and TNF Cytotoxicity Assays—Stable transfectants of L929 cells for expressing the desired proteins were established as described previously (14, 15). Where indicated, L929 cells were electroporated with the above indicated purified *Wox1* construct DNAs (in pEGFP-C1 or pCR3.1), followed by selecting neomycin-resistant stable transfectants or cell colonies using 300 μg/ml G418, an analog of neomycin (Life Technologies, Inc.). Functional analysis of cellular sensitivity to TNF cytotoxicity was performed as described (11–15, 18). The established stable transfectants were cultured on 96-well plates overnight, followed by exposure to recombinant human TNF (Genzyme Corp. (Boston, MA) and R&D Systems (Minneapolis, MN)) for 16–24 h.

Cell Lines—The following cell lines were from American Type Culture Collection (Manassas, VA): murine L929 and NIH/3T3 fibroblasts; human ovarian ME180 and HeLa cells, monocytic U937 and THP-1 cells, transformed 293 fibroblasts, and Molt-4 T cells; neonatal rat H9c2 cardiomyocytes; and monkey kidney COS-7 fibroblasts. The lymphotoxin-producing L929R cells (18), the human neural SK-N-SH cells, and the human breast MCF-7 cells were gifts of Dr. D. Beezhold, R. Aronstam, and J. Noti (Guthrie Research Institute), respectively.

Confocal Microscopy—Where indicated, confocal microscopy analysis was performed to determine the colocalization of WOX1 and mitochondria. Mitochondria were stained by antibodies against cytochrome *c* or by the membrane potential-sensitive mitochondrial stain Mitotracker Red CMXRos (Molecular Probes, Inc., Eugene, OR).

Northern and Western Blotting—To perform Northern hybridization, L929 cells were cultured in 100-mm Petri dishes and treated with hyaluronidase (200 units/ml) for 1–24 h. Total cellular RNAs were isolated from these cells, and Northern hybridization was carried out using 40 μg of RNA/lane (14, 15). Antibodies used in the Western blotting were against IκBα, Bcl-2, Bcl-x_L, p53, a phospho-SAPK/JNK peptide, NF-κB, and α-tubulin (Transduction Laboratories (Lexington, KY) and Santa Cruz Biotechnology (Santa Cruz, CA)). Anti-GFP and anti-cytochrome *c* oxidase subunit 4 (COX4) antibodies were from CLONTECH. Where indicated, images were analyzed by the NIH Image program. Purification of rat liver mitochondrial proteins for Western blotting was performed as described (19).

Yeast Two-hybrid Interactions—The CytoTrap yeast two-hybrid system was from Stratagene. Unlike the traditional system, which depends upon protein-protein interaction in the nucleus (20), this assay system is based on the binding of an Sos-tagged bait protein to a cell membrane-anchored target protein (tagged with a myristoylation signal) that results in activation of the Ras signaling pathway, thereby permitting mutant yeast *cdc25H* to grow at 37 °C using a selective agarose medium or plate containing galactose. Two constructs of *Wox1* as baits (in the pSos vector) and three constructs of p53 as targets (in the pMyr vector) were made (see Table I). Binding interactions using combination of these vectors were performed. Vectors that are included in the system for positive binding interactions are pSos-MafB and pMyr-MafB (21), and those that are included for negative binding interactions are empty pSos and empty pMyr, pMyr and lamin C, or other vectors.

RESULTS

Molecular Cloning of Murine Wox1—To further explore the mechanism whereby hyaluronidase enhances TNF cytotoxicity, we isolated a murine *Wox1* cDNA (2197 bases; GenBank™/EBI accession number AF187014) by differential display and cDNA library screening. The cDNA possesses an open reading frame, a typical Kozak sequence at the initiation site (ATG), and an upstream in-frame stop codon. The deduced murine WOX1 protein sequence (414 amino acids, 46 kDa) possesses two N-terminal WW domains (first domain, amino acids 18–47; and second domain, amino acids 59–87), an NLS (GKRKRV, amino acids 50–55), and a C-terminal short-chain ADH domain (amino acids 121–330) (Fig. 1). WW domains are known to bind proteins with a particular proline motif, (A/P)PP(A/P)Y (22, 23). Whether the WW domains of WOX1 bind to this motif is not known.

The human gene coding for *WOX* cDNAs (or known as *WWOX* or *FOR*) has been mapped to a fragile site on chromosome 16 (24–26). Murine WOX1 is highly homologous to full-length human WWOX (46 kDa) (24) and FOR II (46.7 kDa) (25). Three alternatively spliced variants are FOR I (41.2 kDa), FOR III (21.5 kDa), and FOR IV (4.1 kDa), which possess distinct C-terminal ends (Fig. 1) (25). Two alternatively spliced variants we have identified and sequenced are human prostate WOX3 (identical to FOR III; GenBank™/EBI accession numbers AI669330 and AF187015) (Fig. 1) and FOR I-related human WOX5 (a partial clone; GenBank™/EBI accession number AI219858), whose ADH domain, but not the N terminus, is identical to the sequence of FOR I.

Gene and Protein Expression—Murine L929 fibroblasts constitutively expressed a low level of *Wox1* mRNA, as determined by Northern blotting (Fig. 2*A*). Exposure of L929 cells to hyaluronidase for 2–24 h resulted in increased *Wox1* gene expression (~2.3 kilobases), peaking at 8–24 h (~150% increase) (Fig. 2*A*). The induced *Wox1* gene expression correlates positively with the induction of TNF sensitivity in L929 cells, which requires pretreatment with hyaluronidase for at least 10 h (11–13).

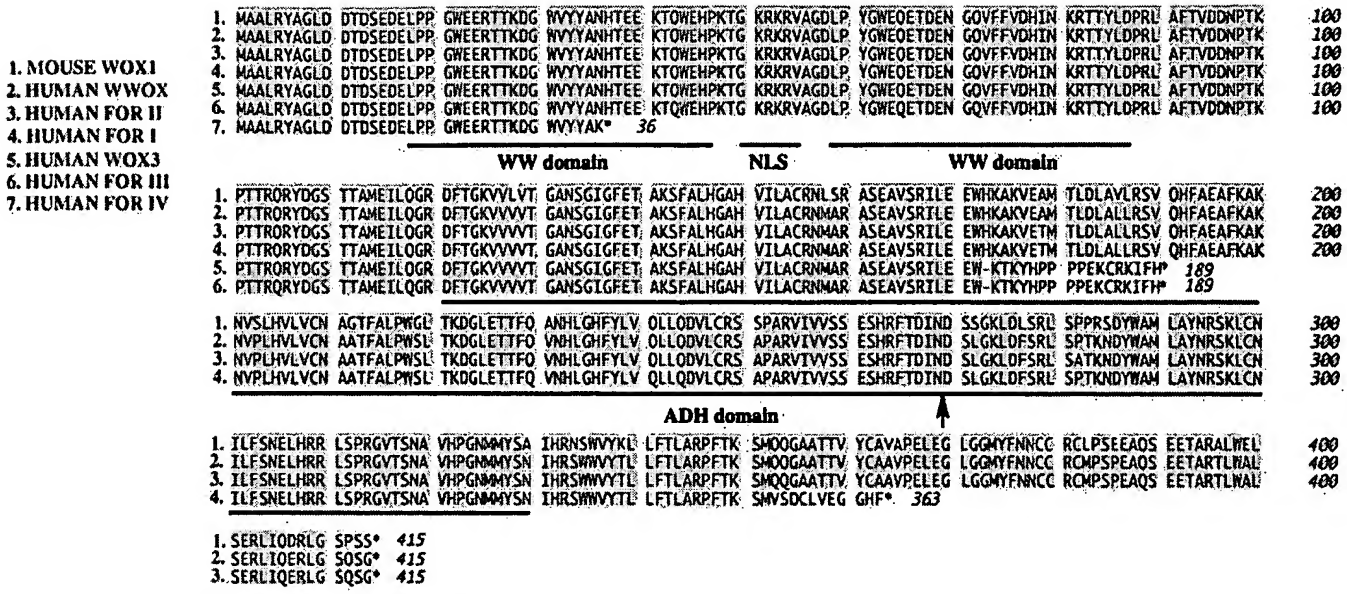

FIG. 1. **Murine and human WW domain-containing oxidoreductase proteins.** The deduced full-length murine WOX1 (GenBank™/EBI accession number AF187014) amino acid sequence (414 amino acids, 46.5 kDa) possesses two N-terminal WW domains (amino acids 18–47 and 59–87; *underlined*), an NLS sequence (amino acids 50–55; *underlined*), and a C-terminal short-chain ADH domain (amino acids 121–330; *underlined*). A putative caspase recognition sequence (DIND, amino acids 267–270) and its cleavage site (*arrow*) are shown. Murine WOX1 is homologous to the following WOX proteins: human WWOX (GenBank™/EBI accession number AF211943) (24); human FOR I (41.2 kDa; accession number AF227526), FOR II (46.7 kDa; accession number AF227527), FOR III (21.5 kDa; accession number AF227528), and FOR IV (4.1 kDa; accession number AF227529) (25); and human WOX3 (accession numbers AI669330 and AF187015). WOX3 is identical to FOR III.

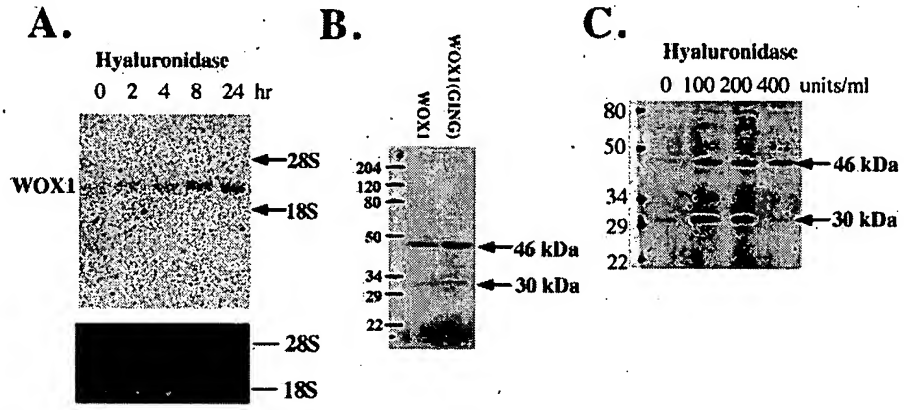

FIG. 2. ***WOX* gene and protein expression.** *A*, exposure of L929 fibroblasts to hyaluronidase (100 units/ml) resulted in a time-dependent increase in *Wox1* gene expression (~150% increase in 8 h; 40 μg of total RNA/lane). *B*, *in vitro* translation of the isolated full-length *Wox1* cDNA (in the pCR3.1 vector) produced a 46-kDa protein and a 30-kDa protein. The 30-kDa protein is probably a degraded protein from 46-kDa WOX1. A putative caspase recognition site (DIND) was altered to a non-caspase recognition sequence (GING), designated *WOX1(GING)*. This alteration failed to prevent the degradation during *in vitro* translation. *C*, stimulation of L929 cells with hyaluronidase (100–200 units/ml) for 24 h resulted in the increased expression of 46- and 30-kDa WOX1 proteins, as determined by Western blotting using antibodies against a synthetic peptide of WOX1 at the N terminus. At high concentrations (>400 units/ml), hyaluronidase suppressed WOX1 expression. The 30-kDa protein is probably a degradation product of 46-kDa WOX1.

As predicted, *in vitro* translation of the full-length murine *Wox1* cDNA produced a protein of ~46 kDa, as analyzed by reducing SDS-polyacrylamide gel electrophoresis (Fig. 2*B*). A 30-kDa product was also observed (Fig. 2*B*). This protein is most likely a degradation product of 46-kDa WOX1 since *Wox1* mRNA, which is derived from the cloned full-length cDNA, is unlikely to undergo alternative splicing.

WOX1 is a single chain protein and does not exist as a dimer, as determined by nonreducing SDS-polyacrylamide gel electrophoresis. A putative caspase recognition site is DIND (267–270). However, this site does not appear to be the proteolytic degradation site. Alteration of the DIND sequence to a non-caspase recognition sequence (GING) by site-directed mutagenesis failed to prevent WOX1 degradation (Fig. 2*B*). The caspase inhibitor peptide acetyl-Asp-Glu-Val-Asp-CHO (aldehyde) at 100–200 μM failed to block WOX1 degradation during *in vitro* translation. Furthermore, the serine protease inhibitors leupeptin and leuhistin at 100 μM could not inhibit WOX1 degradation during *in vitro* translation.

Stimulation of L929 cells with hyaluronidase induced WOX1 protein expression (Fig. 2*C*). Our produced antibodies, which interacted with both human and mouse WOX1, recognized both 46- and 30-kDa WOX1 (Fig. 2*C*). Whether this 30-kDa WOX1 is a degraded protein from 46-kDa WOX1 remains to be determined. Our produced antibodies are specific since the preimmune serum failed to interact with both WOX1 proteins, the synthetic WOX1 peptide blocked the binding of the antibodies to WOX1, and the antiserum also interacted with the *in vitro* translated WOX1 protein (data not shown).

WOX1 Is Mainly Located in the Mitochondria, and TNF Mediates WOX1 Nuclear Translocation—Immunostaining of COS-7 fibroblasts with anti-WOX1 and anti-cytochrome *c* an-

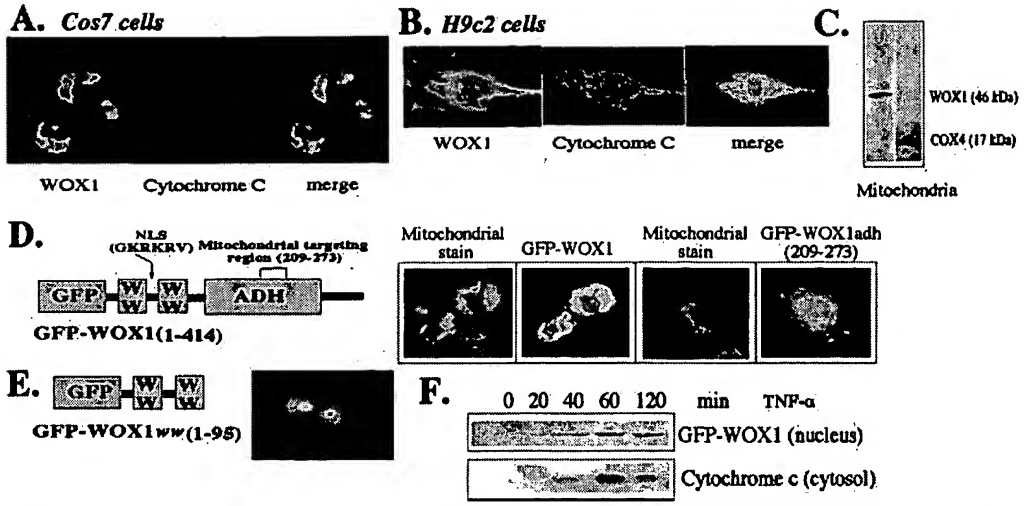

FIG. 3. **WOX1 is mainly present in the mitochondria, and TNF mediates WOX1 nuclear translocation.** *A*, COS-7 cells were stained with both anti-WOX1 and anti-cytochrome *c* antibodies, followed by staining with secondary antibodies, and subjected to confocal microscopy. Colocalization analysis showed that WOX1 is mainly located in the mitochondria and nuclei. *B*, similar results were observed by staining neonatal rat H9c2 cardiomyocytes using both antibodies. *C*, Western blotting showed the presence of WOX1 in the purified rat liver mitochondria. Also, the presence of COX4, a protein on the inner mitochondrial membrane, is regarded as a marker protein for mitochondria. *D*, when expressed in COS-7 cells, the full-length murine GFP-WOX1 protein (construct 2) (Table I) is mainly located in the mitochondria, as analyzed by counterstaining the cells with the membrane potential-sensitive mitochondrial stain MitoTracker Red CMXRos. Protein expression in cells was examined by fluorescent microscopy 24 h post-transfection. Also, by successive deletion and expression analyses, the mitochondrial targeting region was mapped to amino acids 209–273 of the ADH domain (GFP-WOX1adh, construct 7). *E*, however, the truncated GFP-WOX1ww protein (construct 4), which possesses the N-terminal WW domains and the NLS, is present in the nucleus. *F*, stimulation of an established L929 cell line, which constitutively expresses full-length GFP-WOX1 (construct 2), with TNF (20 ng/ml) resulted in the appearance of GFP-WOX1 in the isolated nuclei at the 40-min time point (detected by anti-GFP antibodies). This correlates with the time course of cytochrome *c* release from mitochondria to the cytosol.

tibodies showed the presence of WOX1 in the mitochondria and nuclei, as determined by confocal microscopy and colocalization analysis (Fig. 3*A*). Similar results were observed using neonatal rat heart H9c2 cells (Fig. 3*B*). These results were further confirmed using human ovarian ME180 and HeLa, breast MCF-7, and neural SK-N-SH cells; isolated rat heart cardiomyocytes; and murine NIH/3T3 and L929 cells. The presence of WOX1 in the mitochondria was further confirmed by Western blotting using purified rat liver mitochondria (Fig. 3*C*). COX4 was examined as a marker protein for mitochondria (Fig. 3*C*).

Tagging of full-length murine WOX1 with an N-terminal GFP sequence (construct 2) (Table I) and expression in COS-7 cells revealed the presence of GFP-WOX1 in the mitochondria, as determined 24 h post-transfection (Fig. 3*D*). Mitochondria were stained by the membrane potential-sensitive stain Mitotracker Red CMXRos. Less than 10% of the transfected cells had nuclear localization of this protein.

By making successive deletion constructs (constructs 5–7) (Table I) and expressing these constructs in COS-7 cells, the mitochondrial targeting sequence in WOX1 was mapped within the ADH domain (amino acids 209–273; construct 7) (Fig. 3*D*). The truncated GFP-WOX1ww protein (amino acids 1–95; construct 4), which contains only the N-terminal WW domains and NLS, was expressed in the nucleus (Fig. 3*E*). Similarly, the human prostate GFP-WOX3 protein (see Fig. 1), which possesses the WW domains, the NLS, and a partial ADH domain, was expressed in the nucleus (data not shown).

A time course study showed TNF-mediated GFP-WOX1 nuclear translocation (Fig. 3*F*). This was determined by examining isolated nuclei by Western blotting using an established L929 cell line stably expressing the GFP-WOX1 protein (Fig. 3*F*). This observation correlates with the time point of TNF-mediated cytochrome *c* release from mitochondria to the cytosol in L929 cells (Fig. 3*F*). Similarly, time-dependent endogenous WOX1 protein nuclear translocation was also observed in COS-7 and H9c2 cells upon stimulation with TNF for 20 min (data not shown).

TNF-mediated WOX1 nuclear translocation took at least 20–40 min, which occurred shortly after TNF-mediated p65 NF-κB nuclear translocation (at ~10–15 min), as determined by immunostaining and fluorescent microscopy. Alteration of the NLS sequence (GKRKRV) to a less hydrophilic sequence (GQGTGV) by site-directed mutagenesis (construct 18) abolished the TNF-mediated nuclear translocation of this mutant protein. No nuclear translocation was observed when treating the ADH domain (GFP-WOX1adh, construct 5)-expressing cells with TNF. In parallel with the TNF-mediated mitochondrial permeability transition, treatment of COS-7 cells with atractyloside (2 mM) (27) for 40 min to increase the opening of mitochondrial transition pores also resulted in cytochrome *c* release to the cytosol and WOX1 nuclear translocation (data not shown).

WOX1 Enhances TNF Cytotoxicity by Up-regulation of p53, but Down-regulation of Bcl-2 and Bcl-x_L—To determine the effect of WOX1 on TNF cytotoxic functions, we established several L929 cell lines that stably expressed the above indicated GFP-WOX1 proteins (using constructs 2, 4, and 5). Expression of these proteins was determined by Western blotting using specific antibodies against GFP (Fig. 4*A*). As expected, the protein sizes of the expressed full-length GFP-WOX1 (predicted, 72 kDa; observed, 57 kDa) and GFP-WOX1adh (predicted, 50 kDa; observed, 34 kDa) were reduced by ~15 kDa, probably due to C-terminal degradation. Exposure of these GFP-WOX1 stable transfectants to TNF for 24 h resulted in enhancement of TNF-mediated cell death as compared with control cells transfected with GFP alone (Fig. 4*B*). Both the WW and ADH domains enhanced TNF-mediated L929 cell death (Fig. 4*B*). Expressing untagged full-length WOX1 (construct 1) in L929 cells also increased their TNF sensitivity (data not shown), indicating that GFP does not affect the WOX1 protein function.

In contrast, constitutive expression of antisense *Wox1* mRNA (using construct 3) resulted in cellular resistance to TNF killing (resistance increase by 65–90%). These observations indicate that WOX1 participates in the TNF cytotoxicity pathway.

Although NF-κB is believed to play an essential role in

TABLE I
Polymerase chain reaction primers and expression constructs

Name (construct)	Cloning site	PCR[a] primers (5′ to 3′)	
pCR3.1 (no tag)			
1. WOX1-(1–414) (46 kDa)[b]	T/A	Forward:	GGTGGCGACTCCTGGAGCCCG
		Reverse:	TTTGACACCAGACCAACTGGT
pEGFP-C1 (N-terminal GFP tag)			
2. WOX1-(1–414) (72 kDa)[c]	*Eco*RI	Forward:	AATCGAATTCAATGGCAGCTCTGCGCTAT
		Reverse:	TTCAGAATTCTTAGCTGGATGGACTACC
3. Antisense WOX1-(1–414) (26 kDa GFP)	*Eco*RI	Forward:	AATCGAATTCAATGGCAGCTCTGCGCTAT
		Reverse:	TTCAGAATTCTTAGCTGGATGGACTACC
4. WOX1ww-(1–95) (both WW domains; 37 kDa)	*Eco*RI	Forward:	AATCGAATTCAATGGCAGCTCTGCGCTAT
		Reverse:	TTCAGAATTCTTAGTCCACGGTAAATGCCAA
5. WOX1adh-(180–392) (50 kDa)	*Hind*III/*Bam*HI	Forward:	GCTCAAGCTTCGATGACCCTGGACCTGGCC
		Reverse:	GGTGGATCCTCCTCACTCTGAGCCTCC
6. WOX1adh-(180–273) (36 kDa)	*Eco*RI	Forward:	TCGAATTCTATGACCCTGGACCTGGCC
		Reverse:	CAGAATTCTCACCCGGAGGAGTCATTAATATC
7. WOX1adh-(209–273) (33 kDa)	*Eco*RI	Forward:	TCGAATTCTATGACCTGTAATGCAGGGACGTTT
		Reverse:	CAGAATTCTCACCCGGAGGAGTCATTAATATC
pCDNA3.1 (C-terminal v5 tag)			
8. WOX1-(1–414) (51 kDa)	T/A	Forward:	AATCGAATTCAATGGCAGCTCTGCGCTAT
		Reverse:	GCTGGATGGACTACCCAG
9. WOX1–1ww-(1–60) (first WW domain; 12 kDa)	T/A	Forward:	AATCGAATTCAATGGCAGCTCTGCGCTAT
		Reverse:	CGGCAAATCTCCTGCGAC
10. WOX1–1ww-(1–90) (both WW domains; 16 kDa)	T/A	Forward:	AATCGAATTCAATGGCAGCTCTGCGCTAT
		Reverse:	CAATCTTGGATCCAAGTA
pCDNA3.1/CTGFP (C-terminal GFP tag)			
11. p53-(1–393) (81 kDa)	T/A	Forward:	AAGATGGAGGAGCCGCAGTC
		Reverse:	TTTGTCTGAGTCAGGCCCTTCTGT
pSos (N-terminal Sos tag)			
12. WOX1-(1–414) (172 kDa)	*Mlu*I	Forward:	CGCACGCGTGATGGCAGCTCTGCGCTATGC
		Reverse:	CACGCGTGCGTTAGCTGGATGGACTACC
13. WOX1ww-(1–90) (137 kDa)	*Mlu*I	Forward:	CGCACGCGTGATGGCAGCTCTGCGCTATGC
		Reverse:	CACGCGTGCGTTACAATCTTGGATCCAAGTA
pMyr (N-terminal Myr tag)			
14. p53-(1–393) (55 kDa)	*Eco*RI	Forward:	AGAGAATTCATGGAGGAGCCGCAGTCAG
		Reverse:	AGAGAATTCTCTTCAGTCTGAGTCAGGCCCT
15. p53-(1–110) (14 kDa)	*Eco*RI	Forward:	AGAGAATTCATGGAGGAGCCGCAGTCAG
		Reverse:	AGAGAATTCTCTTCAACGGAAACCGTAGCTGCC
16. p53-(66–110) (14 kDa)	*Eco*RI	Forward:	AGAGAATTCATGCCAGAGGCTGCTCCCC
		Reverse:	AGAGAATTCTCTTCAACGGAAACCGTAGCTGCC

Mutant constructs by site-directed mutagenesis	Mutated sites	Site of interest
17. WOX1(GING)-pCR3.1	D267G and D270G	A putatative caspase cleave site (aa 267–270)
Forward: TTTACAGGTATTAATGGCTCCTCCGGGAAACTT		
Reverse: AAGTTTCCCGGAGGAGCCATTAATACCTGTAAA		
18. WOX1(NLSqgtg)-pEGFP-C	K51Q, R52G, K53T, and R54G	Nuclear localization sequence (aa 50–55)
Forward: ATCTCCTGCGACCCCTGTCCCCTGGCCGGTTTTCGG		

[a] Polymerase chain reaction; aa, amino acids.
[b] Full-length WOX1 is from amino acids 1 to 414, and p53 is from amino acids 1 to 393.
[c] The predicted protein size (protein plus the tag).

blocking cell death by TNF, ionizing radiation, and anticancer drugs (28–33), the WOX1-increased TNF cytotoxicity is not due to impaired NF-κB activation or nuclear translocation. Time course studies showed that the kinetics of TNF-mediated IκBα degradation were similar in both GFP- and GFP-WOX1-expressing L929 cells (Fig. 4*C*). Also, TNF induced NF-κB (p65) nuclear translocation in both cells, as determined by immunostaining and fluorescent microscopy (data not shown). Additionally, TNF rapidly induced SAPK/JNK activation (peaking at 5–20 min) in both GFP-WOX1- and GFP-expressing cells, as determined using anti-phospho SAPK/JNK peptide antibodies in Western blotting. Thus, the involvement of NF-κB and SAPK/JNK in WOX1-increased TNF killing is unlikely.

To exclude the possibility that the WOX1-increased TNF susceptibility in the established L929 transfectants is due to mutation of these cells, transient transfection experiments were performed. Transient expression of TRADD (34), the first adaptor protein recruited by the TNF receptor, in COS-7 fibroblasts resulted in activation of the TNF killing pathway and cell death (Fig. 4*D*). The TRADD-mediated death was significantly enhanced (2–3-fold increase) by WOX1 (using a noncytotoxic concentration) in cotransfection studies (Fig. 4*D*). Similar results were observed with ovarian ME180 and L929 cells (data not shown).

We next examined whether the WOX1-increased TNF killing is associated with down-regulation or up-regulation of apoptosis regulatory proteins. Western blot analysis showed that p53 expression was significantly increased (~200%) in L929 cells stably expressing full-length GFP-WOX1 or the GFP-WOX1adh as compared with cells expressing GFP alone (Fig. 4*E*). Both GFP-WOX1 and GFP-WOX1adh proteins were present in the mitochondria (Fig. 3). In contrast, cells stably expressing nuclear GFP-WOX1ww failed to increase p53 expression (Fig. 4*E*). Notably, the ADH domain significantly suppressed the expression of the apoptosis inhibitors Bcl-2 and Bcl-x_L (>85%), whereas the WW domains had no effect (Fig. 4*E*). IκBα levels in these cells were not changed (Fig. 4*E*). The housekeeping protein α-tubulin was examined as control for protein loading (Fig. 4*E*). These data suggest that enhancement of TNF killing by WOX1 is associated in part with its

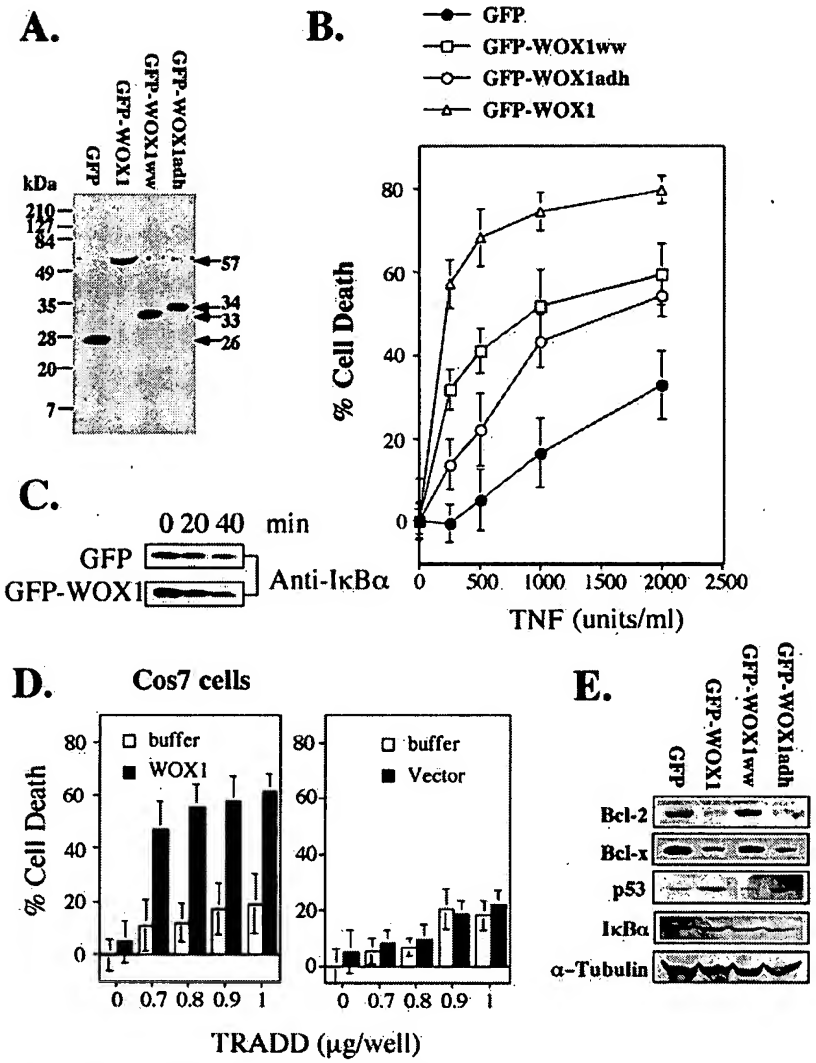

FIG. 4. **WOX1 enhances TNF killing of L929 cells.** *A*, four stable L929 transfectants were established to continuously express full-length GFP-WOX1 (predicted, 72 kDa; observed, 57 kDa) (construct 2), truncated GFP-WOX1ww (predicted, 37 kDa; observed, 33 kDa) (construct 4), truncated GFP-WOX1adh (predicted, 50 kDa; observed, 34 kDa) (construct 5), or GFP protein (26 kDa) alone. A degradation of 15 kDa was observed in the expressed GFP-WOX1 and GFP-WOX1adh proteins. Anti-GFP antibody was used in Western blotting. *B*, exposure of these WOX1-expressing cells to TNF for 24 h resulted in enhancement of cell death as compared with the control GFP-expressing cells (n = 8). *C*, a representative time course study showed that TNF-mediated IκBα degradation was similar in both the GFP-WOX1- and GFP-expressing cells, indicating that WOX1 enhancement of TNF cytotoxicity is not due to impaired IκBα degradation and NF-κB activation. *D*, transfection of COS-7 cells (in 96-well plates) with a *TRADD* cDNA construct (in a cytomegalovirus-based pRK vector) by $CaPO_4$ resulted in cell death in 24 h (*white bars*), and the cell death was significantly enhanced by cotransfection with the full-length murine *Wox1*-pCR3.1 cDNA (0.2 μg/well; construct 1; *black bars*). At this concentration, WOX1 could not mediate cell death. In controls, the empty vector pCR3.1 (0.2 μg/well) failed to increase TRADD-mediated cell death. *E*, down-regulation of Bcl-2 and Bcl-x_L expression and up-regulation of p53 expression were observed in the cells expressing GFP-WOX1 or GFP-WOX1adh, but not in the cells expressing GFP-WOX1ww or GFP alone. Both IκBα and α-tubulin levels were not changed in these cells.

increased p53 expression and reduced expression of Bcl-2 and Bcl-x_L.

WW Domain-mediated Apoptosis Is Independent of Caspases and Serine Proteases—Indeed, transient overexpression of WOX1 in cells mediated death over a 48-h culture period. For instance, the TNF-resistant NIH/3T3 fibroblasts were transfected with the full-length *Wox1* cDNA (construct 1) by $CaPO_4$, and cell death was observed 48-h post-transfection (Fig. 5*A*). The apoptotic cells revealed condensation of cytoplasm and nuclei. Similarly, transient expression of full-length *Wox1* mediated the death of ME180, L929, U937, and other TNF-resistant cells such as 293, L929R, and neonatal rat H9c2 cardiomyocytes (data not shown).

As summarized in Table II, both the ADH (construct 5) and WW (construct 4) domains induced DNA fragmentation when overexpressed in NIH/3T3 cells. As a positive control, overexpression of p53 induced apoptosis. In contrast, both antisense *Wox1* (construct 3) and NLS-mutated WOX1 (NLSqgtg, construct 18) failed to mediate DNA fragmentation. Failure of NLS-mutated WOX1 in inducing apoptosis suggests that nuclear translocation of WOX1 is necessary for inducing cell death. Also, the presence of the WW domains in WOX1 may suppress the apoptosis-inducing activity of the ADH domain.

The WW domain-induced cell death is independent of caspases and serine proteases. Transient expression of the N-terminal WW domains (first and second domains; construct 10) or the first WW domain (construct 9) in NIH/3T3 cells also resulted in cell death 48 h post-transfection (Fig. 5*B*). These proteins contain the NLS, thus expressing in the nuclei. Exposure of the transfected cells to the caspase inhibitors acetyl-Asp-Glu-Val-Asp CHO (aldehyde) and benzyloxycarbonyl-Val-Ala-Asp-fluoromethyl ketone and the serine protease inhibitors leupeptin and leuhistin (100 μM) failed to block cell death (Fig. 5*B*). These results indicate that the WW domain-mediated cell

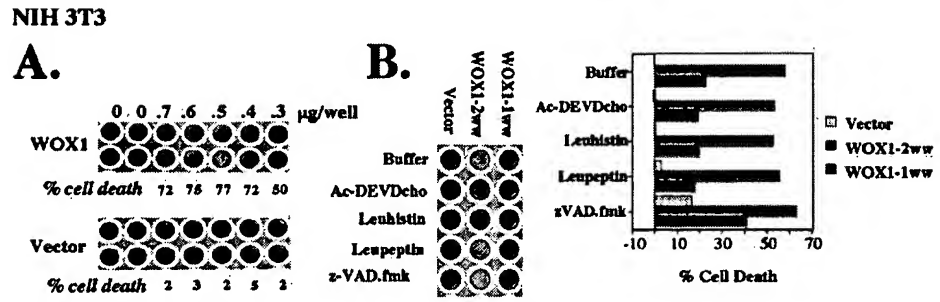

FIG. 5. **WW domain-mediated cell death is independent of caspases and serine proteases.** *A*, transient expression of full-length *Wox1*-pCR3.1 (construct 1) in NIH/3T3 cells resulted in cell death, as observed 48-h post-transfection (by the $CaPO_4$ method), whereas the empty pCR3.1 vector had no effect. The cells were stained by crystal violet. *B*, transient expression of the first and second WW domains (WOX1-2ww-pcDNA3.1, construct 10) or the first WW domain (WOX1-1ww-pcDNA3.1, construct 9) resulted in the death of NIH/3T3 cells. The caspase inhibitors acetyl-Asp-Glu-Val-Asp-cho (*Ac-DEVDcho*) and benzyloxycarbonyl-Val-Ala-Asp-fluoromethyl ketone (*z-VAD.fmk*) (100 μM) and the serine protease inhibitors leuhistin and leupeptin (100 μM) failed to block the WW domain-mediated cell death. The extent of cell death was quantified (*bar graph*). The empty vector-transfected cells (without treatment) were regarded as 0%.

TABLE II
WOX1-mediated DNA fragmentation of NIH/3T3 cells

	Increase in DNA fragmentation	Vector[a]
	%	
Sham	0	None
Empty vector	32	pEGFP-C1
Full-length WOX1	448	2
WOX1adh-(180–392)	312	5
WOX1ww-(1–95)	334	4
WOX1-(NLSqgtg)	31	18
Antisense WOX1	78	3
p53	344	11

[a] See Table I for the vectors. NIH/3T3 cells were transfected with 20 μg of DNA by $CaPO_4$. Forty-eight h post-transfection, the extent of DNA fragmentation was determined and quantified by NIH Image.

death is independent of caspases and serine proteases.

WOX1 and p53 Are Partners in Apoptosis—Since WOX1 increased p53 expression, we then investigated whether p53 is involved in the WOX1-mediated cell death. Transient expression of the WW domains mediated the death of NIH/3T3 cells in 48 h, and the killing function was increased by cotransfection with p53 (Fig. 6, *A*, *panels a* and *b*). Also, using non-killing concentrations of p53 and WOX1 in transfecting monocytic U937 cells (by electroporation), a synergistic killing effect was observed when combining p53 and WOX1 (data not shown).

Notably, antisense expression of WOX1 in NIH/3T3 cells abolished p53-mediated cell death (Fig. 6*A*, *panel c*). Similarly, antisense expression of WOX1 also inhibited p53 apoptosis of THP-1 cells in cotransfection experiments (Fig. 6*B*). These results suggest that there is a partnership between p53 and WOX1 in apoptosis.

However, using p53-deficient NCI-H1299 cells, transient expression of both the WW and ADH domains mediated cytochrome *c* release from mitochondria and cell death, indicating that WOX1-mediated cell death is independent of p53 (Fig. 6*C*). Similar results were observed using full-length WOX1 (data not shown). Together, these data suggest that WOX1-mediated apoptosis is independent of p53, but p53 apoptosis requires the participation of WOX1.

The WW Domains of WOX1 Bind to the Proline-rich Region of p53—Confocal microscopy and colocalization analysis revealed that p53 and WOX1 colocalized in the cytosol and partly in the nuclei in MCF-7 cells (Fig. 7*A*). Similar results were obtained using other cells such as ME180 and COS-7.

Immunoprecipitation of L929 cytosolic lysates with anti-p53 antibodies resulted in coprecipitation of both p53 and WOX1 (Fig. 7*B*), indicating the binding interactions between endogenous p53 and WOX1. The presence of p53 in the precipitates was confirmed using anti-p53 antibodies in Western blotting (data not shown). Stimulation of L929 cells with TNF for 2 h resulted in migration of both proteins to the nuclei (determined by immunostaining) (data not shown) and the disappearance of both proteins from the cytosolic lysates in coprecipitation studies (Fig. 7*B*).

Yeast two-hybrid analysis showed that the proline-rich region of p53 (amino acids 66–110) physically interacts with the WW domains of WOX1 *in vivo* (Fig. 7*C*). In negative controls, no binding interactions were observed using antisense WOX1ww and p53, empty vector (pSos) and empty vector (pMyr), and MafB and lamin C (Fig. 7*C*). MafB self-binding interactions were tested as positive binding controls (Fig. 7*C*).

DISCUSSION

In this study, we cloned and functionally characterized the murine WOX1 protein by antibodies, GFP tagging and expression, and other approaches. The gene encoding WOX1 is located on a fragile chromosomal site (24–26). Homozygous deletion of this gene has been found in various cancers (24–26). Whether WOX1 plays a role in cancer development remains to be established. We determined that WOX1 is located mainly in the mitochondria. Mitochondrial intermembrane space is a reservoir for a variety of apoptogenic proteins such as cytochrome *c*; procaspase-2, -3, and -9; and apoptosis-inducing factor (AIF) (35). Whether WOX1 is present in this intermembrane space remains to be established. Apoptotic stimuli such as TNF and staurosporine induce WOX1 nuclear translocation. WOX1 enhances TNF cytotoxic function via its nuclear targeting WW domains and the mitochondrial targeting ADH domain, suggesting that WOX1 functions at both cytosolic and nuclear levels. Functionally, WOX1 mediates apoptosis when overexpressed. WOX1 binds p53 in the cytosol. WOX1-mediated apoptosis is independent of p53, whereas p53-mediated cell death requires the participation of WOX1. This observation suggests that WOX1 is an essential partner of p53 in apoptosis.

In agreement with other studies (24, 25), *Wox1* mRNA is ubiquitously expressed in most tissues and organs in mouse, as determined by reverse-transcription-polymerase chain reaction (data not shown). Based on the gene structure, four splice variants of WOX proteins are predicted (25). However, we observed additional WOX protein species at high molecular sizes (65 and 100 kDa) in Western blotting using human organs and cell lines (data not shown). Also, three mRNA transcripts probably encoding high molecular mass WOX proteins have been found (25). Indeed, additional splice variants have also been found in the updated expressed sequence tag data base. Accordingly, the functional properties of these proteins remain to be established.

TNF-mediated WOX1 nuclear translocation is independent of the TNF signaling pathway that leads to phosphorylation

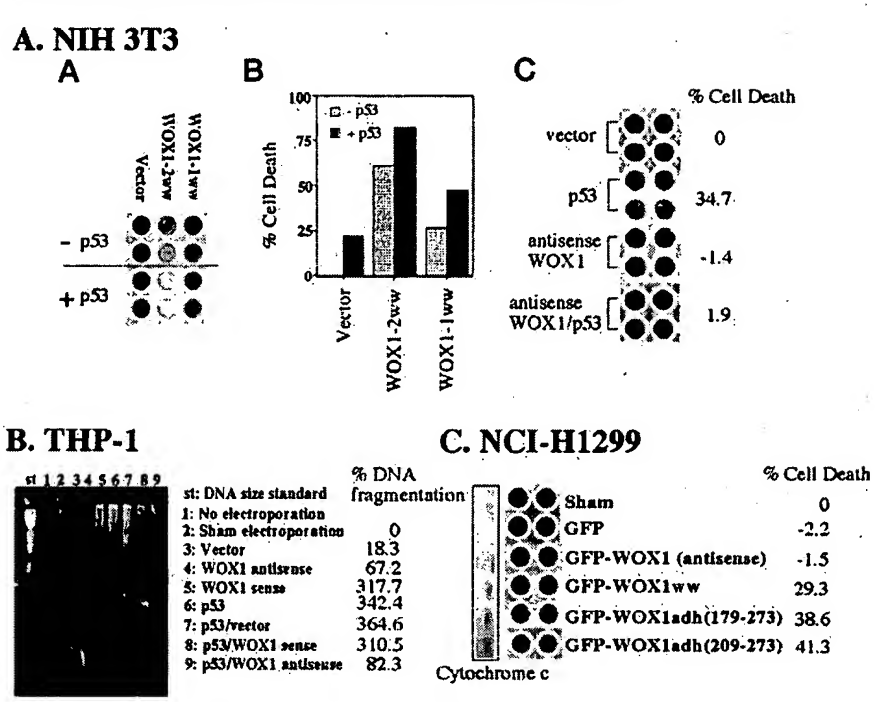

FIG. 6. **p53-mediated apoptosis is blocked by antisense *Wox1*.** *A*, shown in *panel a* is the p53-increased killing of NIH/3T3 cells by WW domains in transient expression experiments (by $CaPO_4$) using constructs of both WW domains (construct 10), the first WW domain (construct 9), and/or p53 (construct 11). The extent of cell death is demonstrated in *panel b* as a *bar graph*. The empty vector-transfected cells are regarded as 0% killing. As shown in *panel c*, blocking of WOX1 expression by antisense mRNA (construct 3) resulted in inhibition of p53-mediated cell death in cotransfection experiments. *B*, as determined by DNA fragmentation assays, inhibition of p53 apoptosis by antisense *Wox1* mRNA was also observed in monocytic THP-1 cells (electroporation with construct 2, 3, or 11 and/or an empty vector). The sham electroporation is regarded as background DNA fragmentation (0%). *C*, nonetheless, in the p53-deficient NCI-H1299 cells, transient expression of both the WW (construct 4) and ADH (constructs 6 and 7) domains mediated cytochrome *c* release and cell death. Similar results were observed using the full-length GFP-WOX1 construct (data not shown). The sham transfection is regarded as 0% killing.

and degradation of IκBα and activation of p65 NF-κB and SAPK/JNK (36–38). For example, the GFP-WOX1-expressing COS-7 cells were pretreated with the proteasome inhibitor benzyloxycarbonyl-Leu-Leu-Leu CHO (aldehyde) (10 μM) to block IκBα degradation or with the IκBα phosphorylation inhibitors Bay 11-7082 and Bay 11-7085 (30 μM) for 1 h, followed by exposure to TNF. These treatments inhibited TNF-mediated p65 NF-κB activation or nuclear translocation, but failed to abolish the GFP-WOX1 nuclear translocation, as determined by immunostaining and fluorescent microscopy (data not shown).

Nonetheless, TNF-mediated WOX1 release from mitochondria could be dependent upon activation of BID (39). TNF mediates cleavage of BID to truncated BID, which translocates to the mitochondria. Truncated BID oligomerizes BAK to generate membrane pores, thus allowing cytochrome *c* and probably WOX1 release. Truncated BID-mediated cytochrome *c* release does not appear to be involved in the opening of mitochondrial transition pores (40). However, atractyloside, an inducer of mitochondrial permeability transition, also induces WOX1 nuclear translocation. This observation suggests that WOX1 release from mitochondria could be dependent upon mitochondrial transition pores as well as BAK oligomerization.

The WW domains of WOX1 are more potent than full-length WOX1 in sensitizing the TNF-resistant COS-7 cells to TNF killing. We found that when COS-7 cells were transiently transfected with the N-terminal WW domains of WOX1 and cultured for 16–24 h, followed by exposure to TNF, these cells underwent nuclear fragmentation in 3 h and subsequent rupture of the cytosolic components and nuclear condensation in 6–16 h. Nonetheless, a prolonged treatment (>12 h) of the full-length WOX1-expressing COS-7 cells with TNF is required to induce cell death.

An intriguing finding in our study is that stable expression of the ADH domain or full-length WOX1 in the mitochondria resulted in down-regulation of Bcl-2 and Bcl-x_L, but up-regulation of p53 in L929 cells. In contrast, the WW domains, when expressed in the nuclei, failed to modulate the expression of these proteins. These results suggest that WOX1 indirectly regulates the expression of p53, Bcl-2, and Bcl-x_L.

The anti-apoptotic Bcl-2 and Bcl-x_L proteins block mitochondrial permeability transition and prevent cytochrome *c* release from mitochondria (41). Bcl-x_L blocks cytochrome *c* release by binding to the anion channel voltage-dependent anion channel on the outer membrane of mitochondria (42). Binding of Bcl-x_L to voltage-dependent anion channel results in closure of the voltage-dependent anion channel. We determined that WOX1 significantly reduces the expression of Bcl-2 and Bcl-x_L in mitochondria. This event may result in opening of the mitochondrial permeability transition pores and release of apoptogenic proteins from the intermembrane space. This notion is supported by the observation that transient overexpression of the ADH domain in cells caused cytochrome *c* release and death.

Another intriguing finding is that when overexpressed, the mitochondrial targeting ADH domain alone (using three regions of the ADH domains; constructs 5–7) was capable of inducing cell death. However, the apoptosis-inducing activity was not found in NLS-mutated full-length WOX1 (construct 18), which indicates that nuclear translocation is needed for the WW domains to mediate cell death. Also, the presence of the mutated WW domains appears to suppress cell death by the ADH domain. Suppression of the ADH domain function is

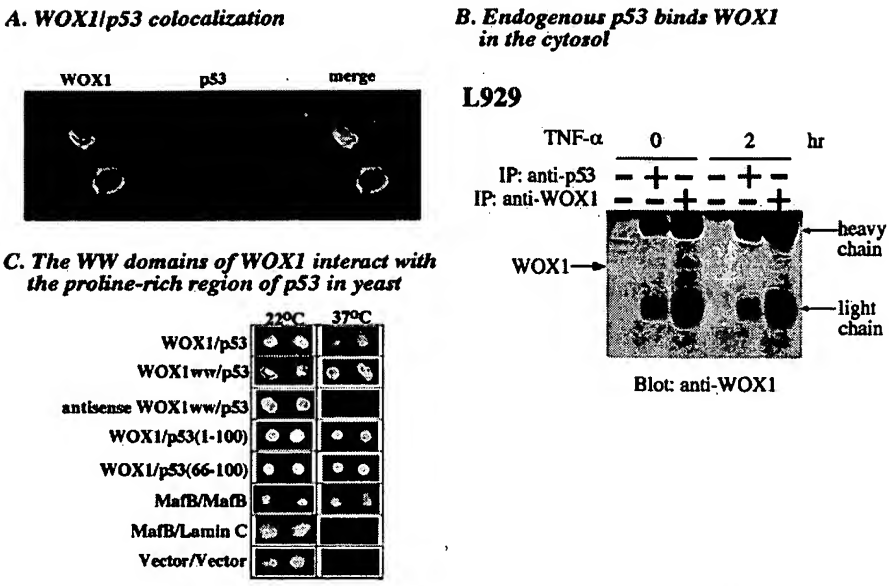

FIG. 7. **p53 and WOX1 colocalization and binding interactions.** *A*, confocal microscopy and colocalization analysis revealed that p53 and WOX1 are colocalized in the cytosol and partly in the nucleus in MCF-7 cells (magnification × 400). *B*, immunoprecipitation (*IP*) of endogenous WOX1 with anti-WOX1 antibodies from the cytosolic lysates of L929 cells, followed by blotting with anti-WOX1 antibodies, revealed the presence of 46-kDa WOX1 (*third lane*). Also, precipitation with anti-p53 antibodies, followed by blotting with anti-WOX1 antibodies, also resulted in the appearance of 46-kDa WOX1 (*second lane*), indicating binding of endogenous p53 to WOX1. In the control without antibodies added, no precipitated protein was observed (*first lane*). Exposure of L929 cells to TNF (20 ng/ml) for 1 h resulted in the disappearance of WOX1 from the cytosol, due to migration of both p53 and WOX1 to the nuclei (*fifth* and *sixth lanes*). *C*, yeast two-hybrid analysis was performed (see "Experimental Procedures"). Interactions between target and bait proteins allow Sos-mediated activation of the Ras signaling pathway, which permits the temperature-sensitive yeast *cdc25H* to grow at 37 °C. Positive binding interactions between full-length p53 (construct 14) and full-length WOX1 (construct 12) or WOX1ww (both WW domains; construct 13) are demonstrated, as evidenced by the growth of yeast at 37 °C. Similar results were obtained with the N-terminal proline-rich region in p53 (amino acids 1–100 and 66–100; constructs 15 and 16, respectively) and full-length WOX1. p53 failed to bind to the antisense construct of WOX1ww (reverse orientation of WOX1ww cDNA). MafB protein self-interaction is a positive control for the assay system. In negative controls, the yeast failed to grow at 37 °C when testing MafB-lamin C or empty vector (pSos)-empty vector (pMyr) interactions. Two representative colonies (out of 15–30) are shown from each binding experiments.

probably related to protein folding when the WW domains are present in the WOX1 protein. Other types of dehydrogenase domain proteins such as AIF (35) and the CC3 protein (43) have been shown to induce cell death when overexpressed.

Endogenous WOX1 colocalizes with p53 in the cytosol. Ectopic expression of both GFP-WOX1 and red fluorescent protein-tagged p53 in COS-7 cells also results in cytosolic colocalization (>50% in p53/WOX1-expressing cells) (data not shown). Co-immunoprecipitation studies further support binding of p53 with WOX1 in the cytosol. Yeast two-hybrid experiments show the binding of the WW domains of WOX1 to the proline-rich region (amino acids 66–110) in p53. Based on these observations, it is reasonable to suggest that both p53 and WOX1 migrate together to the nucleus in response to TNF.

Ectopic expression of p53 and WOX1 showed that both proteins mediate apoptosis in a synergistic manner. Although WOX1 can mediate apoptosis independently of p53, blocking of WOX1 expression by antisense mRNA abolishes p53 apoptosis. The inhibition of p53 apoptosis is not due to blocking of p53 protein synthesis by the antisense *Wox1* mRNA (data not shown). These observations strongly indicate that WOX1 is an essential partner of p53 in apoptosis. The proline-rich region has been shown to be necessary for p53-mediated apoptosis (44). Our data suggest that binding of WOX1 to this region in p53 appears to be essential for p53 apoptosis-inducing activity.

A wide range of transcription factors including c-Jun, AP-2, NF-E2, CAAT/enhancer-binding protein-α, and PEBP2/CBF, contain the WW domain-binding motif (22, 23). Thus, most of the WW domain-containing proteins act as gene transcription activators or coactivators (45, 46). When overexpressed, the WW domains of WOX1 mediate apoptosis. Whether this is related to the transcriptional activation of apoptotic genes by the WW domains of WOX1 remains to be established. Nonetheless, our data show that the WW domains fail to increase p53 protein expression and suppress Bcl-2 and Bcl-x_L expression.

Susin *et al.* (35) isolated mitochondrial AIF, a homolog of bacterial oxidoreductase. Once released from mitochondria, AIF translocates to the nucleus. Although recombinant AIF induces apoptosis of isolated nuclei (35), whether nuclear AIF induces chromatin condensation and nuclear DNA fragmentation *in vivo* is unknown. In response to apoptogenic signals such as staurosporine, both WOX1 and AIF migrate to the nucleus and mediate cell death in a caspase-independent mechanism. TNF induces WOX1 nuclear translocation. Whether AIF migrates to the nucleus in response to TNF is unknown. WOX1 enhances TNF cytotoxicity by increasing the expression of p53 (and probably other pro-apoptotic proteins) as well as suppressing the expression of Bcl-2 and Bcl-x_L. In contrast, AIF does not appear to be involved in the regulation of protein expression. Whether AIF and WOX1 act synergistically in mediating cell death is not known.

Although the TNF signaling pathway that leads to caspase activation and cell death has been well defined, we[2] and others (47) have shown that TNF-mediated cell death cannot be blocked by inhibitors of caspases. This raises the possibility that TNF induces a caspase-independent killing pathway. Data from us and Susin *et al.* (35) support that both WOX1 and AIF are the downstream mediators of the caspase-independent TNF killing pathway.

Finally, a high abundance of WOX1 was observed in rat heart (data not shown). This suggests that WOX1 plays a homeostatic role in this organ. The heart is a TNF-producing

[2] N.-S. Chang, N. Pratt, J. Heath, and L. Schultz, unpublished data.

organ, and TNF plays a key role in the pathogenesis of congestive heart failure (48, 49). Patients with chronic and severe congestive heart failure have increased levels of TNF in the circulation and cardiac tissues. TNF exerts a negative inotropic effect and triggers the apoptotic process in cardiomyocytes. Whether WOX1 plays a major role in the TNF-mediated apoptosis of cardiomyocytes remains to be established.

Acknowledgments—We thank Drs. Derek Strassheim, Samira Khera, and Henry Puhl (Guthrie Research Institute); Dr. Steven P. Tammariello (Binghamton University), Dr. J. E. V. Watson (Imperial Cancer Fund, Edinburgh, United Kingdom), and Dr. R. Richards (Women's and Children's Hospital, North Adelaide, Australia) for carefully reviewing the manuscript. We thank Jeffery Mattison for sequencing analysis and SK-N-SH cells, Dr. D. Goeddel (Tularik Inc.) for the *TRADD* cDNA construct, Drs. D. Beezhold and J. Noti for L929R and MCF-7 cells, Dr. S. Ikeda for rat organs, Dr. R. Richards for the sequences of FOR proteins, and Mrs. Terrie Zimmer for assistance with antibody production.

REFERENCES

1. Lokeshwar, V. B., Lokeshwar, B. L., Pham, H. T., and Block, N. L. (1996) *Cancer Res.* **56,** 651–657
2. Bertrand, P., Girard, N., Duval, C., d'Anjou, J., Chauzy, C., Menard, J. F., and Delpech, B. (1997) *Int. J. Cancer* **73,** 327–331
3. Podyma, K. A., Yamagata, S., Sakata, K., and Yamagata, T. (1997) *Biochem. Biophys. Res. Commun.* **241,** 446–452
4. Tamakoshi, K., Kikkawa, F., Maeda, O., Suganuma, N., Yamagata, S., Yamagata, T., and Tomoda, Y. (1997) *Br. J. Cancer* **75,** 1807–1811
5. Lokeshwar, V. B., Soloway, M. S., and Block, N. L. (1998) *Cancer Lett.* **131,** 21–28
6. Liu, D., Pearlman, E., Diaconu, E., Guo, K., Mori, H., Haqqi, T., Markowitz, S., Willson, J., and Sy, M. S. (1996) *Proc. Natl. Acad. Sci. U. S. A.* **93,** 7832–7837
7. De Maewyer, E., and De Maeyer-Guignard, J. (1992) *Int. J. Cancer* **51,** 657–660
8. Croix, B. S., Rak, J. W., Kapitain, S., Sheehan, C., Graham, C. H., and Kerbel, R. S. (1996) *J. Natl. Cancer Inst.* **88,** 1285–1296
9. Smith, K. J., Skelton, H. G., Turiansky, G., and Wagner, K. F. (1997) *J. Am. Acad. Dermatol.* **36,** 239–242
10. Baumgartner, G., Gomar-Hoss, C., Sakr, L., Ulsperger, E., and Wogritsch, C. (1998) *Cancer Lett.* **131,** 85–100
11. Chang, N.-S. (1997) *Am. J. Physiol.* **273,** C1987–C1994
12. Chang, N.-S. (1998) *Int. J. Mol. Med.* **2,** 653–659
13. Chang, N.-S., Carey, G., Pratt, N., Chu, E., and Ou, M. (1998) *Cancer Lett.* **132,** 45–54
14. Carey, G. B., and Chang, N.-S. (1998) *Biochem. Biophys. Res. Commun.* **249,** 283–286
15. Chang, N.-S., Mattison, J., Cao, H., Pratt, N., Zhao, Y., and Lee, C. (1998) *Biochem. Biophys. Res. Commun.* **253,** 743–749
16. Schultz, J., Milpetz, F., Bork, P., and Ponting, C. P. (1998) *Proc. Natl. Acad. Sci. U. S. A.* **95,** 5857–5864
17. Schultz, J., Copley, R. R., Doerks, T., Ponting, C. P., and Bork, P. (2000) *Nucleic Acids Res.* **28,** 231–234
18. Chang, N.-S. (1995) *J. Biol. Chem.* **270,** 7765–7772
19. Bossy-Wetzel, E., and Green, D. R. (1999) *J. Biol. Chem.* **274,** 17484–17490
20. Bemis, L. T., Geske, F. J., and Strange, R. (1995) *Methods Cell Biol.* **46,** 139–151
21. Kelly, L. M., Englmeier, U., Lafon, I., Sieweke, M. H., and Graf, T. (2000) *EMBO J.* **19,** 1987–1997
22. Bork, P., and Sudol, M. (1994) *Trends Biochem. Sci.* **19,** 531–533
23. Bedford, M. T., Reed, R., and Leder, P. (1998) *Proc. Natl. Acad. Sci. U. S. A.* **95,** 10602–10607
24. Bednarek, A. K., Laflin, K. J., Daniel, R. L., Liao, Q., Hawkins, K. A., and Aldaz, C. M. (2000) *Cancer Res.* **60,** 2140–2145
25. Reid, K., Finnis, M., Hobson, L., Mangelsdorf, M., Dayan, S., Nancarros, J. K., Woollatt, E., Kremmidiotis, G., Gardner, A., Venter, D., Baker, E., and Richards, R. I. (2000) *Hum. Mol. Genet.* **9,** 1651–1663
26. Paige, A. J., Taylor, K. J., Stewart, A., Sgouros, J. G., Gabra, H., Sellar, G. C., Smyth, J. F., Porteous, D. J., and Watson, J. E. (2000) *Cancer Res.* **60,** 1690–1697
27. Fiore, C., Trezeguet, V., Le Saux, A., Roux, P., Schwimmer, C., Dianoux, A. C., Noel, F., Lauquin, G. J., Brandolin, G., and Vignais, P. V. (1998) *Biochimie (Paris)* **80,** 137–150
28. Beg, A. A., and Baltimore, D. (1996) *Science* **274,** 782–784
29. Van Antwerp, D. J., Martin, S. J., Kafri, T., Green, D. R., and Verma, I. M. (1996) *Science* **274,** 787–789
30. Wang, C.-Y., Mayo, M. W., and Baldwin, A. S., Jr. (1996) *Science* **274,** 784–787
31. Mayo, M. W., Wang, C.-Y., Cogswell, P. C., Rogers-Graham, K. S., Lowe, S. W., Der, C. J., and Baldwin, A. S., Jr. (1997) *Science* **278,** 1812–1815
32. Bargou, R. C., Emmerich, F., Krappmann, D., Bommert, K., Mapara, M. Y., Arnold, W., Royer, H. D., Grinstein, E., Greiner, A., Scheidereit, C., and Dorken, B. (1997) *J. Clin. Invest.* **100,** 2961–2969
33. Limuro, Y., Nishiura, T., Hellerbrand, C., Behrns, K. E., Schoonhoven, R., Grisham, J. W., and Brenner, D. A. (1998) *J. Clin. Invest.* **101,** 802–811
34. Hsu, H., Xiong, J., and Goeddel, D. V. (1995) *Cell* **81,** 495–504
35. Susin, S. A., Lorenzo, H. K., Zamzami, N., Marzo, I., Snow, B. E., Brothers, G. M., Mangion, J., Jacotot, E., Costantini, P., Loeffler, M., Larochette, N., Goodlett, D. R., Aebersold, R., Siderovski, D. P., Penninger, J. M., and Kroemer G. (1999) *Nature* **397,** 441–446
36. Liu, Z. G., Hsu, H., Goeddel, D. V., and Karin, M. (1996) *Cell* **87,** 565–576
37. Natoli, G., Costanzo, A., Ianni, A., Templeton, D. J., Woodgett, J. R., Balsano, C., and Levrero, M. (1997) *Science* **275,** 200–203
38. Natoli, G., Costanzo, A., Moretti, F., Fulco, M., Balsano, C., and Levrero, M. (1997) *J. Biol. Chem.* **272,** 26079–26082
39. Wei, M. C., Lindsten, T., Mootha, V. K., Weiler, S., Gross, A., Ashiya, M., Thompson, C. B., and Korsmeyer, S. J. (2000) *Genes Dev.* **14,** 2060–2071
40. Kim, T. H., Zhao, Y., Barber, M. J., Kuharsky, D. K., and Yin, X. M. (2000) *J. Biol. Chem.* **275,** 39474–39481
41. Cai, J., Yang, J., and Jones, D. P. (1998) *Biochim. Biophys. Acta* **1366,** 139–149
42. Shimizu, S., Narita, M., and Tsujimoto, Y. (1999) *Nature* **399,** 483–487
43. Whitman, S., Wang, X., Shalaby, R., and Shtivelman, E. (2000) *Mol. Cell. Biol.* **20,** 583–593
44. Zhu, J., Zhang, S., Jiang, J., and Chen, X. (2000) *J. Biol. Chem.* **275,** 39927–39934
45. Komuro, A., Saeki, M., and Kato, S. (1999) *Nucleic Acids Res.* **27,** 1957–1965
46. Yagi, R., Chen, L. F., Shigesada, K., Murakami, Y., and Ito, Y. (1999) *EMBO J.* **18,** 2551–2562
47. Vercammen, D., Beyaert, R., Denecker, G., Goossens, V., Van Loo, G., Declercq, W., Grooten, J., Fiers, W., and Vandenabeele, P. (1998) *J. Exp. Med.* **187,** 1477–1485
48. Torre-Amione, G., Kapadia, S., Lee, J., Durand, J. B., Bies, R. D., Young, J. B., and Mann, D. L. (1996) *Circulation* **93,** 704–711
49. Meldrum, D. R. (1998) *Am. J. Physiol.* **274,** R577–R595

Inhibition of the p53 Tumor Suppressor Gene Results in Growth of Human Aortic Vascular Smooth Muscle Cells

Potential Role of p53 in Regulation of Vascular Smooth Muscle Cell Growth

Motokuni Aoki, Ryuichi Morishita, Hidetsugu Matsushita, Shin-ichiro Hayashi, Hironori Nakagami, Kei Yamamoto, Atsushi Moriguchi, Yasufumi Kaneda, Jitsuo Higaki, Toshio Ogihara

Abstract—Loss of activity of the p53 tumor suppressor gene product has been postulated in the pathogenesis of human restenosis. Although the antioncogenes p53 and retinoblastoma (Rb) susceptibility gene have been reported to play a pivotal role in cell cycle progression in various cells, the role of p53 and Rb in the growth of human vascular smooth muscle cells (VSMC) has not yet been clarified. We used antisense strategy against p53 and Rb genes by the viral envelope–liposomal method. Transfection of antisense p53 oligodeoxynucleotides (ODN) alone resulted in an increase in DNA synthesis compared with control ($P<0.01$). Similarly, transfection of antisense Rb ODN alone resulted in a higher DNA synthesis rate than control ($P<0.01$). Moreover, increase in VSMC number was only induced by transfection of antisense p53 ODN alone or cotransfection of p53/Rb ODN ($P<0.01$), whereas a single transfection of antisense Rb ODN had little effect on cell number. Therefore, we hypothesized that this discrepancy is due to the induction of apoptosis mediated by p53. Interestingly, apoptotic cells were markedly increased in VSMC transfected with antisense Rb ODN alone, accompanied by the induction of p53 protein. The number of apoptotic cells was attenuated by cotransfection of antisense p53 ODN ($P<0.01$). We finally examined the molecular mechanisms of apoptosis induced by the absence of Rb. In VSMC transfected with antisense Rb ODN, bax, a promoter of apoptosis, was significantly increased in VSMC transfected with antisense Rb ODN ($P<0.01$), whereas bcl-2 and Fas did not play a pivotal role in the induction of apoptosis. Overall, these data first demonstrated that the antioncogenes p53 and Rb negatively regulated the cell cycle in VSMC, suggesting that the modulation of their activity may mediate VSMC growth such as that in restenosis and atherosclerosis. The presence of p53 plays a pivotal role in the regulation of apoptosis in human VSMC growth, probably through the bax pathway. These results provide evidence that p53 is a functional link between cell growth and apoptosis in VSMC. (***Hypertension.* 1999;34:192-200.**)

Key Words: antisense ■ genes ■ apoptosis ■ restenosis ■ muscle, smooth, vascular

Intimal hyperplasia is the pathological process that underlies restenosis, atherosclerosis, and vascular graft occlusion; it develops in large part as a result of vascular smooth muscle cell (VSMC) proliferation and migration induced by a complex interaction of multiple growth factors that are activated by vascular injury.[1] The process of VSMC proliferation is dependent on the coordinated activation of a series of cell cycle regulatory genes that results in mitosis. A critical element of cell cycle progression regulation involves the complex formed by E2F, cyclin A, and cdk 2.[2] The dissociation of the transcription factor E2F from this complex is proposed to play a pivotal role in the regulation of cell proliferation by inducing the coordinated transactivation of genes involved in cell cycle regulation. The importance of cell cycle regulation is apparently great, because we and others have previously reported the successful prevention of restenosis after angioplasty with antisense oligodeoxynucleotides (ODN) against cell cycle regulatory genes, decoy cis element of E2F binding site, and gene transfer of nonphosphorylated Rb (retinoblastoma gene).[3–6] Therefore, research has focused on the role of antioncogenes in the regulation of VSMC growth. In particular, p53 (p53 tumor suppressor gene) and Rb have been postulated to negatively regulate the cell cycle in various cell types.[7–9] However, little is known about the role of p53 and Rb in the regulation of VSMC. The presence of a functional p53 protein has been implicated as a critical determinant to regulate DNA replication, DNA repair, and programmed cell death.[7,9–11] On the other hand, the antiproliferative effect of the Rb product has also been reported to depend on its capacity to bind to E2F and thereby

Received February 9, 1999; first decision March 4, 1999; revision accepted April 6, 1999.

From the Department of Geriatric Medicine (M.A., H.M., S.H., H.N., K.Y., A.M., J.H., T.O.) and Division of Gene Therapy Science (R.M., Y.K.), Osaka University Medical School, Suita, Japan.

Correspondence to Ryuichi Morishita, MD, PhD, Division of Gene Therapy Science, Osaka University Medical School, 2-2 Yamada-oka, Suita 565, Japan.

Hypertension is available at http://www.hypertensionaha.org

prevent this transcription factor from binding to the E2F cis element within the promoters of the essential cell cycle regulatory genes.[7-10] Therefore, the abnormal progression of the cell cycle seen in cancer is thought to result from the mutation of these negative cell cycle regulatory genes, especially p53 and Rb.[7-9] Of importance, recent studies suggested that loss of p53 activity may be responsible for the pathogenesis of human restenosis.[12-14] From this viewpoint, it is necessary to understand the negative regulation of the cell cycle by p53 and Rb in human VSMC. This study examines the role of p53 and Rb in negative regulation of the cell cycle in human VSMC with the use of antisense strategy.

Methods

Cell Culture

Human aortic VSMC (passage 5) were obtained from Clonetics Corp (San Diego, Calif) and cultured in modified MCDB131 medium supplemented with 5% fetal calf serum, 100 U/mL penicillin, 100 mg/mL streptomycin, 10 ng/mL epidermal growth factor, 2 ng/mL basic fibroblast growth factor, and 1 mmol/L dexamethasone in the standard fashion.[15] All the cells were used within passages 5 to 6.

Synthesis of ODN and Selection of Target Sequences

The sequences of phosphorothioate ODN against human p53 and Rb were as previously reported[16,17]: (Rb antisense: 5′-GTG-AAC-GA*C*-*ATC*-TCA-TCT-AGG-3′; Rb sense: 5′-CCT-AGA-TGA-G*AT*-*GTC*-GGT-CAC-3′; p53 antisense: 5′-CGG-CTC-CTC-*CAT*-GGC-AGT-3′; p53 sense: 5′-ACT-GCC-*ATG*-GAG-GAG-CCG-3′; scrambled Rb: 5′-AGC-TAG-CTA-GCT-AGC-TAG-CTA-3′; scrambled p53: 5′-AGT-GGC-CTG-CAT-CTC-CGC-3′; antisense thrombomodulin: 5′-ACC-CAG-AAA-GAA-AAT-CCC-3′. These antisense ODN inhibit human p53 and Rb synthesis in human hematopoietic cells.[16,17] We also used scrambled ODN (5′-CGT-CGT-CGG-TAC-CGT-CCA-3′) as negative control.

Preparation of Hemagglutinating Virus of Japan Liposomes

Phosphatidylserine, phosphatidylcholine, and cholesterol were mixed in a weight ratio of 1:4.8:2.[3-5] Dried lipid was hydrated in 200 μL balanced salt solution (BSS) (137 mmol/L NaCl, 5.4 mmol/L KCl, 10 mmol/L Tris-HCl, pH 7.6) containing sense or antisense ODN. The control liposome complex contained BSS without ODN. Purified hemagglutinating virus of Japan (HVJ) (Z strain) was inactivated by UV irradiation (110 ergs/mm^2 per second) for 3 minutes just before use. The liposome suspension was mixed with HVJ (20 000 hemagglutinating units). The mixture was incubated at 4°C for 10 minutes and then for 60 minutes with gentle shaking at 37°C. Free HVJ was removed from the HVJ liposomes by sucrose density gradient centrifugation. The top layer of the sucrose gradient was collected for use.

Effect of Antisense ODN on DNA Synthesis

VSMC were seeded onto 96-well tissue culture plates. At 80% confluence, VSMC were rendered quiescent by incubation for 48 hours in defined serum-free medium (DSF) supplemented with insulin (5×10^{-7} mol/L), transferrin (5 mg/mL), and ascorbate (0.2 mmol/L).[18] Then 10 μL HVJ liposomes (containing 15 μmol/L ODN) was added to the wells. The cells were incubated at 4°C for 10 minutes and then at 37°C for 30 minutes. The cells were washed 3 times with BSS containing 2 mmol/L $CaCl_2$ and incubated in DSF for 16 hours. Relative rates of DNA synthesis were assessed by determination of ^{3}H-thymidine incorporation into trichloroacetic acid–precipitable material over the next 24 hours after 16 hours of incubation.[19]

Counting of Cell Number

Human aortic VSMC were seeded onto uncoated 96-well tissue culture plates (Corning). After cells reached 80% confluence, the medium was changed to fresh DSF. The cells were then incubated for 48 hours. Then transfection of ODN was performed as described above. On day 1, the medium was again changed to fresh DSF containing 0.05% fetal bovine serum (GIBCO). After 3 days, an index of cell proliferation was determined with a water soluble tetrazolium (WST) cell counting kit (Wako).[20] Briefly, 50 000 cells per well reflects absorbance of 1 for the manufacturer's recommended conditions. The sensitivity of the WST assay is double that of the 3-(4,5-dimethyl-thiazole-2-yl)-2,5-diphenyl-tetrazolium bromide (MTT) assay. For our experimental conditions, an increase in absorbance of 0.2 reflects increase in cell number from 20 000 cells per well.

Counting of Apoptotic Cells

As an assay of cell death by apoptosis, we used fluorescent DNA-binding dyes to define nuclear chromatin morphological features as a quantitative index of apoptosis within the cell culture system. Cells to be analyzed for apoptosis were stained with Hoechst 33342 and propidium iodide and viewed under fluorescence microscopy as previously described.[21-24] The use of both membrane-permeable (H33342) and -impermeable (PI) dyes in the assay allowed the determination of cell viability and plasma membrane integrity and an accounting of any nonapoptotic toxic or necrotic death induced in the study groups. Cells were seeded onto 6-well dishes (Laboratory-Tek) and were cultured in DSF for 2 days after subconfluence. Transfection procedures were as described above. To stain the cells for DNA, they were incubated with Hoechst 33342 (5 μg/mL in PBS) for 20 minutes at 37°C.[23] Individual nuclei were visualized at ×400 to distinguish the normal uniform nuclear pattern from the characteristic condensed coalesced chromatin pattern of apoptotic cells. To quantify apoptosis, 400 nuclei from random microscopic fields were analyzed by an observer blinded to the treatment groups.

In addition, we used the measurement of cellular DNA fragmentation with a cellular DNA fragmentation ELISA kit (Boehringer Mannheim) to quantity apoptosis induced by antisense ODN.[25] Briefly, measurement of 10 000 apoptotic cells per well reflects absorbance of 1.5 for the manufacturer's recommended conditions. The sensitivity of DNA fragmentation ELISA assay is well correlated with the results from the conventional ^{3}H-thymidine–based DNA fragmentation assay. For our experimental conditions, increase in absorbance of 0.2 reflects increase in cell number from 2000 apoptotic cells per well.

Western Blot

Western blot was performed for analysis of Rb, p53, bax, and bcl-2 proteins. VSMC were seeded onto 10-cm dishes. VSMC were grown to confluence and made quiescent by incubation in DSF before transfection. Seventy-two hours after transfection, the cells were fixed with 10% trichloroacetic acid in saline, followed by extraction of total protein with urea-TX (9 mol/L urea, 2% Triton-X, and 5% 2-mercaptoethanol). Samples containing 100 μg protein were run on 7.5% (Rb) or 12.5% (p53, bax, and bcl-2) sodium dodecyl sulfate polyacrylamide gels. Proteins were separated by SDS-PAGE, transferred to nitrocellulose membrane (Hybond ECL, Amersham), and incubated with a monoclonal antibody to Rb (1:500; Pharmingen), p53 (1:20; Calbiochem), bax (1:100; Calbiochem), or bcl-2 (1:100; DAKO) at 4°C overnight. To quantify and compare levels of proteins, the density of each band was measured by densitometry (Shimazu). Amounts of loaded proteins were equal, as confirmed by the staining with Coomassie brilliant blue R (Sigma). Staining with Coomassie brilliant blue R revealed identical protein amounts in all samples of Western blotting. Western blotting of tubulin with the use of anti-tubulin antibody (anti-human mouse IgG; 1:100; Oncogene) was also performed to confirm the equal amounts of loaded proteins.

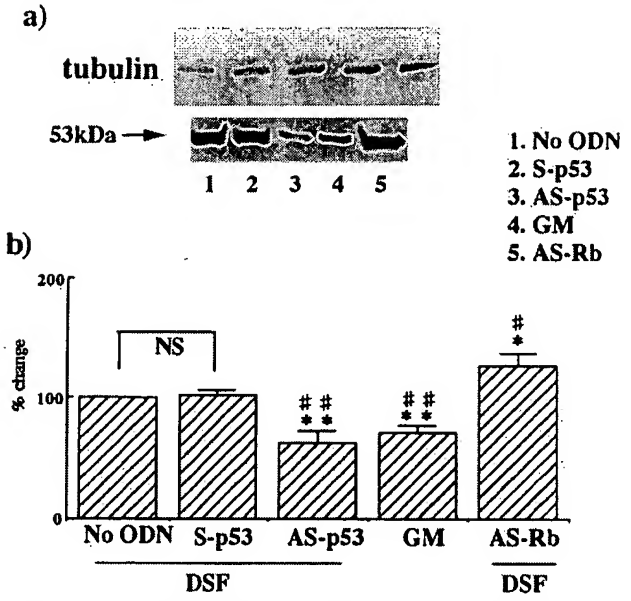

Figure 1. a, Typical example of Western blot of p53 and tubulin proteins in VSMC transfected with antisense p53 or Rb ODN. b, Percent changes in protein level of p53 in VSMC transfected with antisense p53 or Rb ODN. No ODN indicates untransfected VSMC in DSF; S-p53, VSMC transfected with sense p53 ODN in DSF; AS-p53, VSMC transfected with antisense p53 ODN in DSF; GM, untransfected VSMC in growth medium (5% serum); and AS-Rb, VSMC transfected with antisense Rb ODN in DSF. The values were summed from 5 independent experiments. $^{**}P<0.01$, $^{*}P<0.05$ vs 1; $\#\#P<0.01$, $\#P<0.05$ vs 2.

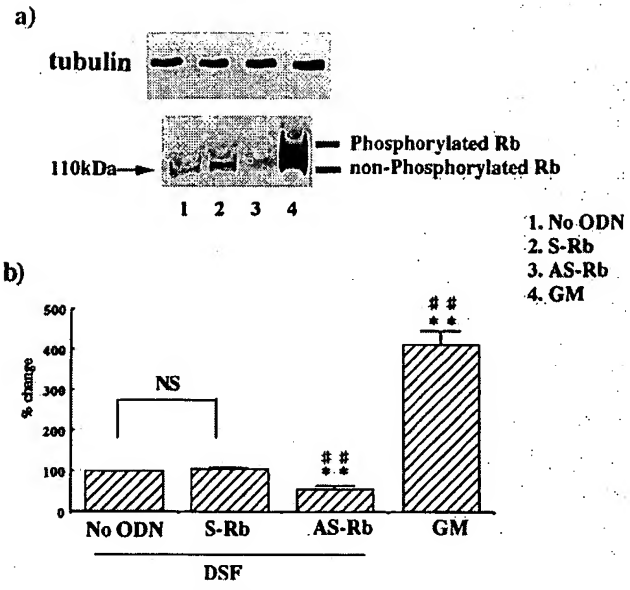

Figure 2. a, Typical example of Western blot of Rb and tubulin proteins in VSMC transfected with antisense Rb ODN. b, Percent changes in protein level of Rb in VSMC transfected with antisense Rb ODN. No ODN indicates untransfected VSMC in DSF; S-Rb, VSMC transfected with sense Rb ODN in DSF; AS-Rb, VSMC transfected with antisense Rb ODN in DSF; and GM, untransfected VSMC in growth medium (5% serum). The values were summed from 5 independent experiments. $^{**}P<0.01$ vs 1; $\#\#P<0.01$ vs 2.

Flow Cytometry

For the detection of proliferating cell nuclear antigen (PCNA) expression by flow cytometry, cells were first fixed at −10°C for 5 minutes in paraformaldehyde-lysine-periodate fixation solution 2 days after transfection. After removal from the fixation solution, cells were washed in PBS and incubated with PCNA monoclonal antibody for 30 minutes at 4°C, washed in PBS, and incubated with fluorescent isothiocyanate–conjugated rabbit anti-mouse IgG monoclonal antibody (DAKO, High Wycombe, England) for 20 minutes at 4°C. An irrelevant IgG1 monoclonal antibody was used in parallel as an isotopic control (Oncogene Science, Cambridge, England) before incubation with the conjugated secondary antibody. Flow cytometric analysis was performed on a FACScan flow cytometer. The assessment of cellular DNA content was also made with a flow cytometer. The cell cycle distribution data were obtained with the use of the Rectangle-Fit (R-FIT) mathematical algorithm of the FACScan/Cellfit software program in the standard manner. Expression of Fas in human aortic VSMC was also examined by flow cytometry with the use of anti-Fas antibody (anti-mouse IgM; Tago).

Statistical Analysis

All values are expressed as mean±SEM. ANOVA with subsequent Scheffé's test was used to determine the significance of differences in multiple comparisons. $P<0.05$ was considered significant.

Results

Effect of Antisense p53 and Rb ODN in Human VSMC

Initially, we examined the presence of products of p53 and Rb genes in human aortic VSMC. As shown in Figures 1 and 2, the presence of p53 and Rb protein in human aortic VSMC was confirmed by Western blot. Therefore, we tested whether transfection of antisense p53 and Rb ODN into VSMC has effects on human VSMC growth. Transfection of either antisense p53 ODN alone or antisense Rb ODN alone or cotransfection of antisense p53 and Rb ODN (p53/Rb ODN) resulted in a significant increase in DNA synthesis assessed by ^{3}H-labeled thymidine incorporation (Table). Increase in DNA synthesis in VSMC transfected with antisense p53 ODN alone and p53/Rb ODN was significantly higher than that with antisense Rb ODN alone ($P<0.01$). In contrast, transfection of scrambled ODN did not alter DNA synthesis (data not shown). The specificity of antisense p53 ODN was confirmed by the observation that the marked decrease in p53

Stimulatory Effect of Antisense p53 and/or Rb ODN in Growth of Human VSMC

Treatment	Thymidine Incorporation, cpm (n=6)	No. of VSMC, Absorbance at 450 nm (n=8)
No ODN	824±102	0.355±0.019
Sense Rb ODN	810±97	0.365±0.021
Antisense Rb ODN	1602±101*‡	0.359±0.028
Sense p53 ODN	786±121	0.337±0.015
Antisense p53 ODN	2205±251†§‖	0.437±0.024†§¶
Sense Rb and p53 ODN	749±121	0.354±0.012
Antisense Rb and p53 ODN	2685±354†§¶	0.440±0.017†§¶
10% serum	4203±475†§¶	0.666±0.016†§¶

*$P<0.05$ vs respective sense ODN.
†$P<0.01$ vs respective sense ODN.
‡$P<0.05$ vs no ODN.
§$P<0.01$ vs no ODN.
‖$P<0.05$ vs antisense Rb ODN.
¶$P<0.01$ vs antisense Rb ODN.

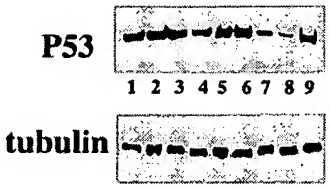

Figure 3. Western blot of p53 and tubulin proteins in VSMC transfected with antisense p53 ODN. 1, VSMC transfected with antisense thrombomodulin ODN in DSF; 2, VSMC cotransfected with sense p53 and sense Rb ODN in DSF; 3, VSMC transfected with scrambled Rb ODN in DSF; 4, VSMC transfected with sense Rb ODN in DSF; 5, VSMC transfected with scrambled p53 ODN in DSF; 6, VSMC transfected with sense p53 ODN in DSF; 7, untransfected VSMC in growth medium (5% serum); 8, VSMC transfected with antisense p53 ODN in DSF; and 9, untransfected VSMC in DSF.

protein was only observed by transfection of antisense p53 ODN but not sense p53, scrambled p53, sense Rb, scrambled Rb, the combination of sense p53 and sense Rb ODN, and thrombomodulin antisense ODN (Figure 3). Marked decrease in p53 mRNA was also observed by the transfection of antisense p53 ODN but not sense p53 ODN, scrambled p53, sense Rb ODN, and antisense thrombomodulin ODN as assessed by Northern blotting (data not shown). The specificity of antisense Rb ODN was also confirmed by the observation that transfection of antisense Rb ODN into quiescent VSMC resulted in a decreased level of Rb protein (Figure 2). In contrast, transfection of sense Rb ODN, transfection of scrambled Rb ODN, cotransfection of sense p53 and sense Rb ODN, and transfection of antisense thrombomodulin ODN did not affect the level of Rb protein (Figures 2 and 4). It is noteworthy that in VSMC transfected with antisense Rb ODN, p53 protein was significantly increased compared with VSMC transfected with sense ODN (Figure 1). Protein of p21 (WAF1/SDI1) that was induced by p53 gene was also decreased in VSMC transfected with antisense p53 ODN (sense p53, 100%; scrambled p53, 104±2%; antisense p53 ODN, 63±5%; $P<0.01$ for antisense p53 ODN versus sense p53 and scrambled p53 ODN).

Next, we examined the number of VSMC to investigate whether an increase in DNA synthesis stimulates cell growth. Of importance, transfection of antisense p53 ODN and antisense p53/Rb ODN resulted in a significant increase in number of VSMC compared with respective sense ODN–transfected VSMC, whereas there was no significant difference in VSMC number between VSMC transfected with antisense Rb ODN and sense Rb ODN (Table). In contrast, there was no significant change in number of VSMC and DNA synthesis transfected with sense p53 ODN, scrambled p53 ODN, sense Rb ODN, scrambled Rb ODN, sense p53/Rb ODN, or antisense thrombomodulin ODN. Moreover, the stimulatory effects of antisense p53 ODN on VSMC growth occurred in a dose-dependent manner, as shown in Figure 5. In contrast, transfection of neither sense p53 ODN, scrambled p53 ODN, nor antisense thrombomodulin ODN stimulated VSMC growth (data not shown).

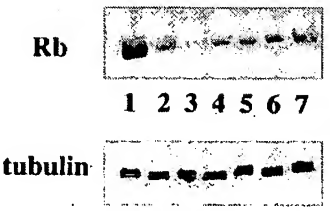

Figure 4. Western blot of Rb and tubulin proteins in VSMC transfected with antisense Rb ODN. 1, Untransfected VSMC in growth medium (5% serum); 2, untransfected VSMC in DSF; 3, VSMC transfected with antisense Rb ODN in DSF; 4, VSMC transfected with sense Rb ODN in DSF; 5, VSMC transfected with scrambled Rb ODN in DSF; 6, VSMC cotransfected with sense p53 and sense Rb ODN in DSF; and 7, VSMC transfected with antisense thrombomodulin ODN in DSF.

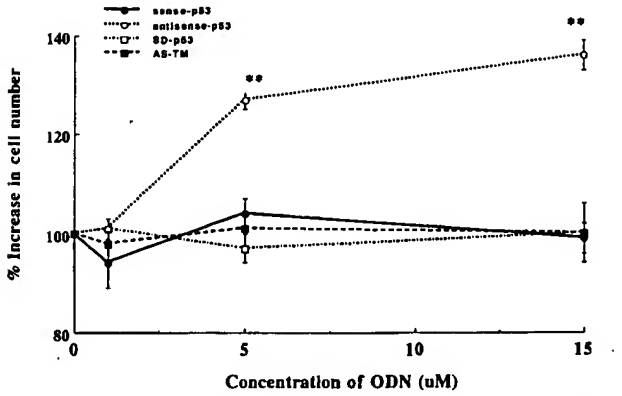

Figure 5. Dose-dependent stimulatory effects of antisense p53 ODN on the number of VSMC. sense-p53 indicates VSMC transfected with sense p53 ODN in DSF; antisense-p53, VSMC transfected with antisense p53 ODN in DSF; SD-p53, VSMC transfected with scrambled p53 ODN in DSF; and AS-TM, VSMC transfected with antisense thrombomodulin ODN in DSF. Each group contains 8 samples. $^{**}P<0.01$ vs other groups. Values are expressed as percent increase in cell number compared with untransfected VSMC.

To confirm that antisense p53 and Rb ODN promoted cell cycle progression of VSMC, the cell cycle of VSMC transfected with antisense ODN was also analyzed by flow cytometry. PCNA-positive VSMC, as a marker of entry into the S phase, were markedly increased in cells transfected with antisense p53 ODN or antisense Rb ODN compared with sense ODN–transfected cells (Figure 6b), consistent with results on DNA synthesis. Transfection of sense p53 ODN, scrambled p53 ODN, sense Rb ODN, and antisense thrombomodulin ODN did not alter the cell cycle. As shown in Figure 6c, progression of the cell cycle into S and G_2/M phases was also confirmed in VSMC transfected with antisense p53 ODN or antisense Rb ODN. These results demonstrated that transfection of either antisense p53 ODN or antisense Rb ODN resulted in cell cycle progression into the G_2/M phase. However, there is a discrepancy between the increase in DNA synthesis and absence of increase in VSMC number in cells transfected with antisense Rb ODN alone. Cell cycle progression by antisense p53 ODN was also supported by the phosphorylation of Rb. As shown in Figure 7, phosphorylated Rb was clearly observed in VSMC transfected with antisense p53 ODN, whereas this occurred with neither sense p53 ODN nor scrambled p53 ODN.

Apoptosis in VSMC Transfected With Antisense Rb ODN

To investigate the mechanisms of this discrepancy, we have focused on the role of p53, because p53 has been postulated

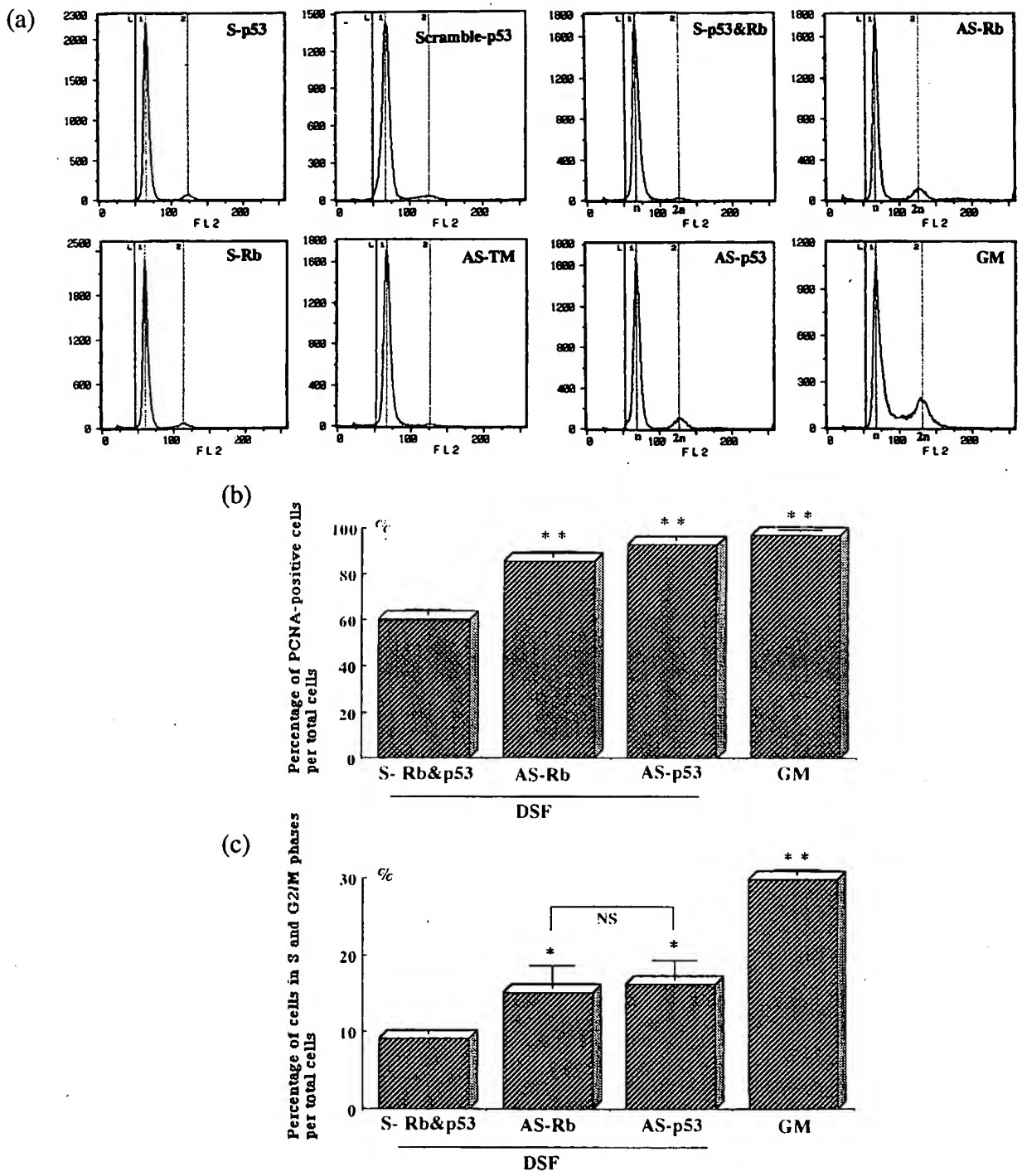

Figure 6. a, Flow cytometry of VSMC transfected with antisense p53 or Rb ODN. b, Stimulatory effect of antisense p53 and Rb ODN on PCNA-positive VSMC assessed by fluorescence-activated cell sorter. c, Effect of antisense p53 and Rb ODN on VSMC number in S and G_2/M phases assessed by fluorescence-activated cell sorter. S-p53 indicates VSMC transfected with sense p53 ODN in DSF; Scramble-p53, VSMC transfected with scrambled p53 ODN in DSF; S-Rb, VSMC transfected with sense Rb ODN in DSF; AS-TM, VSMC transfected with antisense thrombomodulin ODN in DSF; S-Rb&p53, VSMC cotransfected with sense p53 and Rb ODN in DSF; AS-p53, VSMC transfected with antisense p53 ODN in DSF; AS-Rb, VSMC transfected with antisense Rb ODN in DSF; and GM, untransfected VSMC in growth medium (5% serum). $^{**}P<0.01$, $^{*}P<0.05$ vs S-Rb&p53. Each group contains 8 samples.

to regulate programmed cell death, as discussed earlier. Given the cell cycle progression into the G_2/M phase by transfection of antisense Rb ODN alone, it is not likely that the lack of increase in the number of VSMC lacking Rb ODN is due to the cell cycle progression into the S phase but not to the G_2/M phase. Therefore, we hypothesized that the presence of p53 mediated programmed cell death in VSMC transfected with antisense Rb ODN alone. As shown in Figure 8a to 8c, the number of apoptotic cells assessed by nuclear staining was significantly increased by transfection of antisense Rb ODN alone compared with sense ODN. Of importance, cotransfection of antisense p53 and Rb ODN attenuated the

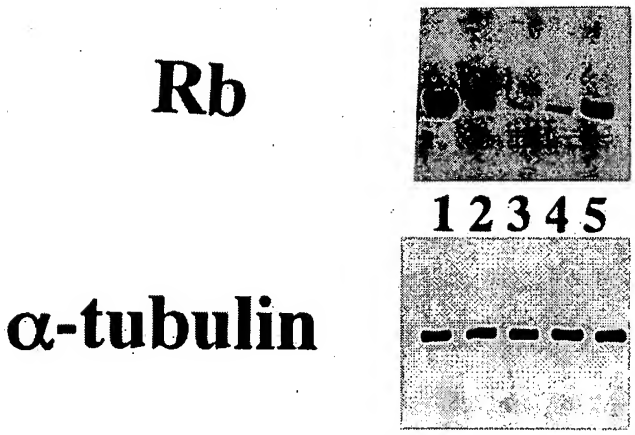

Figure 7. Typical example of Western blot of Rb and tubulin proteins in VSMC transfected with antisense p53 ODN. 1, Untransfected VSMC in growth medium (5% serum); 2, VSMC transfected with scrambled p53 ODN in DSF; 3, VSMC transfected with antisense Rb ODN in DSF; 4, VSMC transfected with sense p53 ODN in DSF; and 5, transfected VSMC with antisense p53 ODN in DSF.

increase in number of apoptotic cells (Figure 8d). In contrast, transfection of sense p53 ODN, scrambled p53 ODN, and sense Rb ODN did not increase the apoptotic cells (sense p53, 6.7±1.5%; scrambled p53, 6.2±1.4%; sense Rb, 6.3±1.2%; antisense Rb, 21.7±5.2%; $P<0.01$ for antisense Rb versus other groups). These results demonstrated the presence of p53-induced apoptosis in VSMC lacking Rb protein by antisense Rb ODN. These results were confirmed by the measurement of DNA fragmentation (Figure 9). Consistent with nuclear staining, DNA fragmentation in VSMC transfected with antisense Rb ODN was significantly increased compared with that in VSMC transfected with sense ODN in a time-dependent manner ($P<0.01$). Increased DNA fragmentation was also significantly attenuated by cotransfection of antisense p53 ODN ($P<0.05$). The specificity of apoptosis induced by antisense Rb ODN was also supported by the observation that there was no significant difference in DNA fragmentation rate at 4 days after transfection among VSMC transfected with sense p53 ODN, scrambled p53 ODN, and sense Rb ODN (sense p53, 0.280±0.016; scrambled p53, 0.295±0.016; sense Rb, 0.276±0.017; antisense Rb, 0.428±0.038 absorbance; $P<0.01$ for antisense Rb versus other groups).

Molecular Mechanisms of Apoptosis in VSMC Transfected With Antisense Rb ODN

Because p53 regulates apoptosis in bcl-2, antiapoptotic gene, dependent pathway, and independent pathway, levels of bcl-2 and bax were measured by Western blot. As shown in Figure 10, bax protein was significantly increased in VSMC transfected with antisense Rb ODN compared with sense Rb ODN ($P<0.01$). More importantly, upregulation of bax induced by transfection of Rb antisense ODN was significantly abolished by cotransfection of p53 antisense ODN. In contrast, as shown in Figure 11, transfection of antisense Rb ODN alone into VSMC also resulted in an increase in bcl-2 protein compared with sense Rb ODN. The ratio of bax to bcl-2 was significantly increased in VSMC transfected with antisense

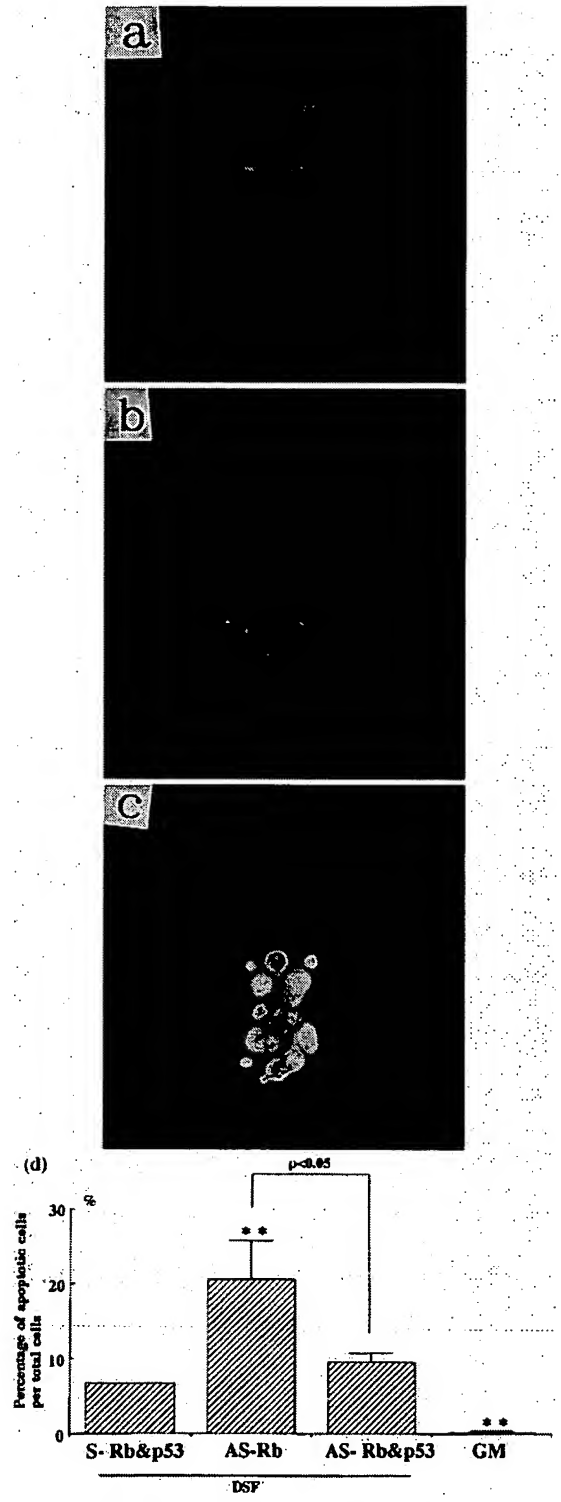

Figure 8. a through c, Typical example of apoptotic cells in VSMC transfected with antisense Rb ODN. a, No apoptotic changes were observed in VSMC treated with 5% serum. b, Morphological apoptotic cells with nuclear condensation after transfection of antisense Rb ODN. c, Morphological apoptotic cells with nuclear fragmentation after transfection of antisense Rb ODN. d, Number of apoptotic cells in VSMC transfected with antisense Rb ODN. S-Rb&p53 indicates VSMC cotransfected with sense p53 and Rb ODN in DSF; AS-Rb, VSMC transfected with antisense Rb ODN in DSF; AS-Rb&p53, VSMC cotransfected with antisense Rb and p53 ODN in DSF; and GM, untransfected VSMC in growth medium (5% serum). **P vs S-Rb&p53. Values are expressed as percentage of apoptotic cells of total cell number. Each group contains 8 samples.

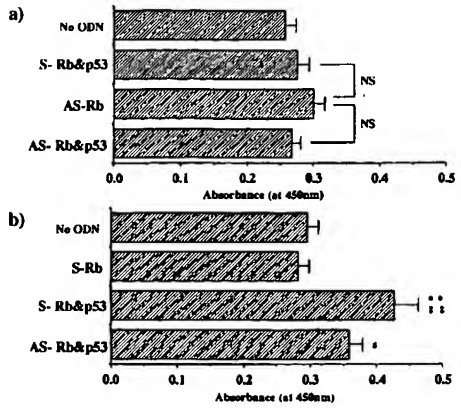

Figure 9. DNA fragmentation expressed as absorbance units in VSMC transfected with antisense Rb ODN and p53 ODN, assessed by ELISA, at 2 (a) and 4 (b) days after transfection. No ODN indicates untransfected VSMC in DSF; S-Rb&p53, VSMC cotransfected with sense Rb and p53 ODN in DSF; AS-Rb, VSMC transfected with antisense Rb ODN in DSF; and AS-Rb&p53, VSMC cotransfected with antisense Rb and p53 ODN in DSF. $^{**}P<0.01$ vs No ODN; ‡‡$P<0.01$ vs No ODN; #$P<0.05$ vs S-Rb&p53. Each group contains 8 samples.

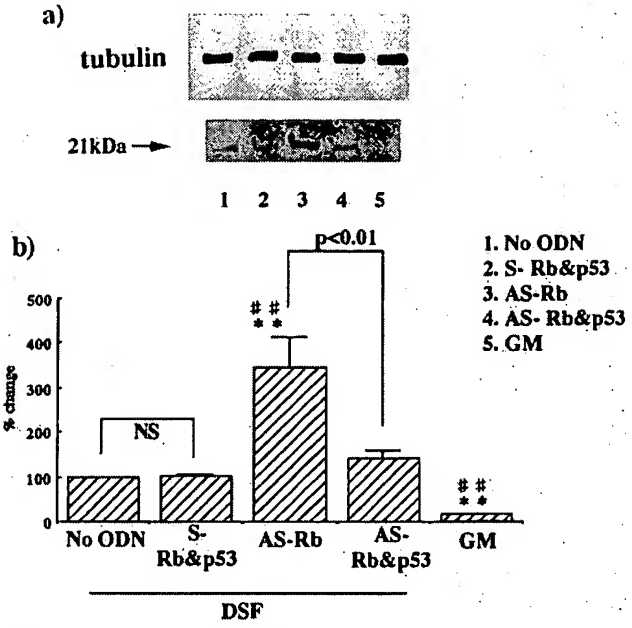

Figure 10. a, Typical example of Western blot of bax and tubulin proteins in VSMC transfected with antisense p53 or Rb ODN. b, Percent changes in protein level of bax in VSMC transfected with antisense p53 or Rb ODN. No ODN indicates untransfected VSMC in DSF; S-Rb&p53, VSMC cotransfected with sense Rb and p53 ODN in DSF; AS-Rb, VSMC transfected with antisense Rb ODN in DSF; AS-Rb&p53, VSMC cotransfected with antisense Rb and p53 ODN in DSF; and GM, untransfected VSMC in growth medium (5% serum). The values were summed from 5 independent experiments. $^{**}P<0.01$ vs 1; ##$P<0.01$ vs 2.

Rb ODN ($P<0.01$, Figure 12), possibly leading to apoptosis. Of importance, consistent with the increased number of apoptotic VSMC, the increase in the ratio of bax to bcl-2 was significantly attenuated by cotransfection with antisense p53 ODN, in addition to antisense Rb ODN ($P<0.05$). We also measured the expression of Fas, a death factor, in VSMC treated with antisense Rb ODN. However, transfection of antisense Rb ODN did not affect Fas expression compared with sense Rb ODN, as assessed by flow cytometry (data not shown).

Discussion

A fundamental pathological feature of vascular disease is marked by the abnormal accumulation of cells within the intimal space, resulting in neointimal lesion formation produced by alterations in the homeostatic balance between cell growth and cell death.[1] One successful approach is to target components of the common pathways that are shared by many growth factors. On the basis of this concept, we have reported that local delivery of antisense ODN directed against cell cycle regulatory genes and ODN containing the E2F cis element sequence as "decoys" inhibited neointimal formation in several models of vascular lesion formation.[3–6] These results emphasize the importance of cell cycle regulation in the disease process. In contrast, negative regulation of the cell cycle is thought to be controlled by antioncogenes in many cell types. Because p53 and Rb have been reported to play a pivotal role in the regulation of cell growth,[2,7,8] frequent mutations in these genes cause a break of cell cycle control, resulting in the neoplastic transformation in human cancers. Given that loss of p53 activity induced by cytomegaloviral infection might be related to the pathogenesis of restenosis,[12–14] it is important to understand the negative cell cycle regulation in human VSMC. Therefore, we used a "loss of function" approach, with antisense ODN, to clarify the roles of p53 and Rb.

The present results showed that single transfection of antisense p53 ODN and cotransfection of p53/Rb ODN promoted DNA synthesis and growth of VSMC, whereas single transfection of antisense Rb ODN resulted in increased DNA synthesis but not number of VSMC (Table). The specificity of antisense ODN was supported by several observations: (1) the decrease in p53 or Rb protein level only by antisense p53 or antisense Rb ODN (Figures 1, 3, 4, and 5); (2) the decrease in p53 mRNA by antisense p53 ODN (Figure 2); (3) the decrease in p21 protein, an inducible protein by p53, by antisense p53 ODN; (4) the lack of response to either sense or scrambled ODN on DNA synthesis (Table); and (5) the lack of response to either sense or scrambled ODN on cell number (Table). Although we thought that transfection of antisense Rb ODN alone promoted cell cycle progression into the S phase but not the G_2/M phase, our initial hypothesis was not supported by flow cytometry, which demonstrated that transfection of either antisense p53 ODN alone or antisense Rb ODN alone promoted cell cycle progression into both S and G_2/M phases (Figure 6). Although the present study demonstrated negative control of the cell cycle by Rb in human VSMC, loss of Rb function is not enough to stimulate human VSMC growth. In contrast, loss of p53 activity in human aortic VSMC is sufficient to promote cell growth.

Because regulation of the intimal cell population requires a delicate balance between cell influx, cell growth, and cell death,[1] we hypothesized that cells lacking Rb undergo cell death/apoptosis, resulting in no change in net balance of cell number

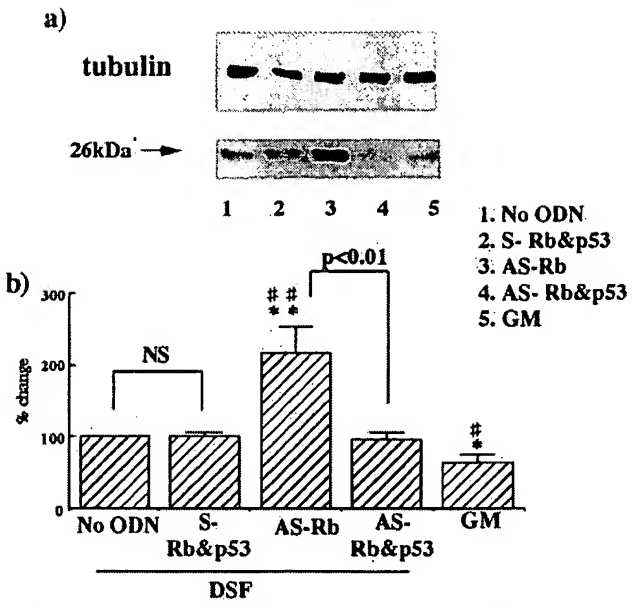

Figure 11. a, Typical example of Western blot of bcl-2 and tubulin proteins in VSMC transfected with antisense p53 or Rb ODN. b, Percent changes in protein level of bcl-2 in VSMC transfected with antisense p53 or Rb ODN. Abbreviations are as defined in Figure 10. The values were summed from 5 independent experiments. $^{**}P<0.01$, $^{*}P<0.05$ vs 1; $\#\#P<0.01$, $\#P<0.05$ vs 2.

despite cell cycle progression. It has become increasingly clear that the process of cell death by apoptosis is a relatively ubiquitous phenomenon observed in a variety of cell types, including VSMC.[26–29] Indeed, recent studies suggest that apoptosis occurs within the context of atherosclerosis and restenosis after angioplasty.[27–29] These phenomena were also confirmed in experimental animals, demonstrating that cell death by apoptosis appears to occur during the processes of vascular remodeling and lesion formation.[30,31] Therefore, p53-mediated apoptosis demonstrated in this study is important in understanding the regulation of VSMC growth, because p53 is known to regulate DNA replication, DNA repair, and programmed cell death.[7,9,10] The evidence of apoptosis induced by p53 in cells lacking Rb was supported by several observations: (1) the increase in apoptotic cells by antisense Rb ODN alone (Figure 8); (2) the increase in DNA fragmentation by antisense Rb ODN alone (Figure 9); and (3) the increase in number of apoptotic cells and DNA fragmentation that was abolished by cotransfection of antisense p53 ODN (Figures 8 and 9). The present data were consistent with the previous observation by Bennett et al[32] that both disruption of Rb/E2F and inhibition of p53 are required for plaque VSMC to proliferate without apoptosis. In this study, we used antisense strategy, whereas Bennett et al used retroviral constructs expressing dominant-negative Rb and p53 genes to explore the interplay of these pathways. Moreover, our finding that p53 was upregulated in cells lacking Rb supports the previous finding that the ablation of Rb enhances apoptosis and overexpression suppresses apoptosis.[32] Consistently, abnormally extensive apoptosis was detected in Rb-deficient mice.[33] On the other hand, overexpression of E2F-1 gene resulted in escape from G_0 into S phase, yet it also initiated p53-dependent apoptosis.[34] Probably the inappropriate entry into the S phase, such as through loss of Rb and release of E2F, in the absence of survival factors may be associated with the activation of apoptosis in the presence of functional p53. In contrast, no increase in VSMC proliferation has been observed in p53 and Rb knockout mice.[33] The findings from knockout mice seem to be different from those of the present study. This discrepancy between knockout mice and the present study is probably due to counterregulatory mechanisms during the developmental stage.

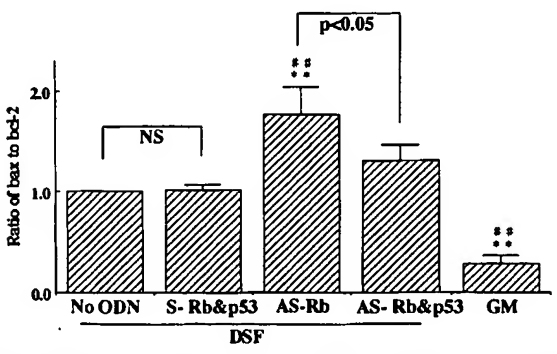

Figure 12. Ratio of bax to bcl-2 in VSMC transfected with antisense Rb ODN and p53 ODN at 4 days after transfection. Abbreviations are as defined in Figure 10. Each group contains 5 samples. $^{**}P<0.01$ vs No ODN; $\#\#P<0.01$ vs S-Rb&p53.

One of the functions of p53 is to repress expression of bcl-2 gene, which exhibits an antiapoptotic action through a cis-acting p53 negative-response element located in the 5′-untranslated region.[35] However, apoptosis in VSMC transfected by antisense Rb ODN observed in this study is unlikely through the bcl-2 pathway, because upregulation of bcl-2 protein was observed in cells lacking Rb. Recently, p53 has also been reported as a direct transcriptional activator of bax gene, which is a homologous protein of bcl-2 gene but which attenuated bcl-2 function.[36] Bcl-2 and bax are homologous proteins that have opposing effects on cell life and death, with bcl-2 serving to prolong cell survival and bax acting as an accelerator of apoptosis.[37] The bcl-2 and bax proteins can form heterodimers in cells.[37] Of importance, transfection of antisense Rb ODN resulted in a significant increase in bax expression in the presence of p53, leading to the significant increase in the ratio of bax to bcl-2 in VSMC that lack Rb. Apoptosis observed in this study may be mediated through the p53-bax pathway. The previous finding that VSMC from atherosclerotic plaques showed a higher number of apoptotic cells than normal VSMC despite the stable expression of bcl-2 gene suggests the presence of an independent apoptotic pathway from bcl-2 gene in human VSMC.[22] Our data may explain the mechanisms of apoptosis observed in such atherosclerotic plaques and restenosis lesions. Consistent with our data, Bennett et al[38] also reported that bcl-2 probably does not play a major role in regulation of apoptosis in VSMC. On the other hand, Fas, another death factor, may not be related to the apoptosis induced by antisense Rb ODN, because transfection of antisense Rb ODN did not affect Fas expression. Because it was previously reported that apoptosis of rat VSMC is regulated by p53-dependent and -independent pathways,[38] other mechanisms might be involved in the

apoptosis of VSMC. Furthermore, the sensitivity of apoptosis induced by p53 may be different among the species of VSMC (p53-sensitive human and rabbit VSMC and p53-resistant rat VSMC).[39]

Overall, these data first demonstrated that p53 and Rb negatively regulate the cell cycle in human aortic VSMC, suggesting that modulation of their activity may mediate VSMC growth such as that in restenosis after angioplasty and atherosclerosis. The product of p53, rather than Rb, may play a pivotal role in the regulation of apoptosis in abnormal human VSMC growth. Further studies of p53 and Rb in the pathological conditions in vascular disease may provide new insights into therapeutic strategies.

Acknowledgments

This study was supported in part by grants from the Uehara Memorial Foundation, the Hoan-sya Foundation, the Japan Cardiovascular Research Foundation, a Japan Heart Foundation research grant, a grant-in-aid from the Tokyo Biochemical Research Foundation, and a grant-in-aid from the Ministry of Education, Science, Sports, and Culture. Dr Morishita is the recipient of a Harry Goldblatt Award from the Council of High Blood Pressure, American Heart Association. We wish to thank Chihiro Noguchi for excellent technical assistance.

References

1. Gibbons GH, Dzau VJ. The emerging concept of vascular remodeling. *N Engl J Med.* 1994;30:1431–1438.
2. Weintraub SJ, Prater CA, Dean DC. Retinoblastoma protein switches the E2F site from positive to negative element. *Nature.* 1992;358:259–261.
3. Morishita R, Gibbons GH, Ellison KE, Nakajima M, Zhang L, Kaneda Y, Ogihar T, Dzau VJ. Single intraluminal delivery of antisense cdc 2 kinase and PCNA oligonucleotides results in chronic inhibition of neointimal hyperplasia. *Proc Natl Acad Sci U S A.* 1993;90:8474–8478.
4. Morishita R, Gibbons GH, Ellison KE, Nakajima M, Leyen HVL, Zhang L, Kaneda Y, Ogihara T, Dzau VJ. Intimal hyperplasia after vascular injury is inhibited by antisense cdk 2 kinase oligonucleotides. *J Clin Invest.* 1994;93:1458–1464.
5. Morishita R, Gibbons GH, Horiuchi M, Ellison KE, Nakajima M, Zhang L, Kaneda Y, Ogihara T, Dzau VJ. A novel molecular strategy using cis element "decoy" of E2F binding site inhibits smooth muscle proliferation in vivo. *Proc Natl Acad Sci U S A.* 1995;92:5855–5859.
6. Chang MW, Barr E, Seltzer J, Jiang YQ, Nabel GJ, Nabel EG, Parmacek MS, Leiden JM. Cytostatic gene therapy for vascular proliferative disorders with a constitutively active form of the retinoblastoma gene product. *Science.* 1995;267:518–522.
7. Vogelstein B, Kinzler KW. P53 function and dysfunction. *Cell.* 1992;70: 523–526.
8. Nevins JR. E2F: a link between the Rb tumor suppressor protein and viral oncoproteins. *Science.* 1992;258:424–429.
9. Lane DP. p53, guardian of the genome. *Nature.* 1992;258:15–16.
10. Symonds H, Krall L, Remington L, Saenz-Robles M, Lowe S, Jacks T, Dyke TV. p53-dependent apoptosis suppresses tumor growth and progression in vivo. *Cell.* 1994;78:703–711.
11. El-Deiry WS, Tokino T, Velculescu VE, Levy DB, Parsons R, Trent JM, Lin D, Mercer WE, Kinzeler KW, Vogelstein B. WAF 1, a potential mediator of p53 tumor suppression. *Cell.* 1993;75:817–825.
12. Speir E, Modali R, Huang ES, Leon MB, Shawl F, Finkel T, Epstein SE. Potential role of human cytomegalovirus and p53 interaction in coronary restenosis. *Science.* 1994;265:391–394.
13. Tsai HL, Kou GH, Chen SC, Wu CW, Lin YS. Human cytomegalovirus immediate-early protein IE2 tethers a transcriptional repression domain to p53. *J Biol Chem.* 1996;271:3534–3540.
14. Zhou YF, Leon MB, Waclawiw MA, Popma JJ, Yu ZX, Finkel T, Epstein SE. Association between prior cytomegalovirus infection and the risk of restenosis after coronary atherectomy. *N Engl J Med.* 1996;335:624–630.
15. Bonin PD, Leadley RJ, Erickson LA. Growth factor-induced modulation of endothelial-1 binding to human smooth muscle cells. *J Cardiovasc Pharmacol.* 1993;22:S125–S127.
16. Bi S, Lanza F, Goldman JM. The involvement of "tumor suppressor" p53 in normal and chronic myclogenous leukemia hemopoiesis. *Cancer Res.* 1994;54:582–586.
17. Hatzfeld J, Li ML, Brown EL, Sookdeo H, Levesque JP, O'Toole TM, Gurney C, Clark SC, Hatzfeld A. Release of early human hematopoietic progenitors from quiescence by antisense transforming growth factor β1 or Rb oligonucleotides. *J Exp Med.* 1991;174:925–929.
18. Libby P, O'Brien KV. Culture of quiescent arterial smooth muscle cells in a defined serum-free medium. *J Cell Physiol.* 1983;115:217–223.
19. Morishita R, Gibbons GH, Pratt RE, Tomita N, Kaneda Y, Ogihara T, Dzau VJ. Autocrine and paracrine effects of atrial natriuretic peptide gene transfer on vascular smooth muscle and endothelial cellular growth. *J Clin Invest.* 1994;94:824–829.
20. Ishiyama M, Shiga M, Sasamoto K, Mizoguchi M, He P. A new sulfonated tetrazolium salt that produces a highly water-soluble formazan dye. *Chem Pharm Bull (Tokyo).* 1993;41:1118–1122.
21. Bennett MR, Evan GI, Newby AC. Deregulated expression of the c-myc oncogene abolishes inhibition of proliferation of rat vascular smooth muscle cells by serum reduction, interferon-gamma, heparin, and cyclic nucleotides analogues and induces apoptosis. *Circ Res.* 1994;74:525–536.
22. Bennett MR, Schwartz SM. Apoptosis of human vascular smooth muscle cells derived from normal vessels and coronary atherosclerotic plaques. *J Clin Invest.* 1995;95:2266–2274.
23. Pollman MJ, Yamada T, Horiuchi M, Gibbons GH. Vasoactive substances regulate vascular smooth muscle cell apoptosis: countervailing influences of nitric oxide and angiotensin II. *Circ Res.* 1996;79:748–756.
24. Aoki M, Morishita R, Matsushita H, Nakano N, Hayashi S, Tomita N, Yamamoto K, Moriguchi A, Higaki J, Ogihara T. Serum deprivation induced apoptosis accompanied by up-regulation of p53 and bax in human aortic vascular smooth muscle cells. *Heart Vessels.* 1997;S12: 71–75.
25. Ito M, Watanabe M, Ihara T, Kamiya H, Sakurai M. Fas antigen and bcl-2 expression on lymphocytes cultured with cytomegalovirus and varicella-zoster virus antigen. *Cell Immunol.* 1995;160:173–177.
26. Raff M. Social controls on cell survival and cell death. *Nature.* 1992; 356:397–400.
27. Isner JM, Kearney M, Bortman S, Passeri J. Apoptosis in human atherosclerosis and restenosis. *Circulation.* 1995;91:2703–2711.
28. Geng YJ, Libby P. Evidence for apoptosis in advanced human atheroma: colocalization with interleukin-1-β-converting enzyme. *Am J Pathol.* 1995;147:251–266.
29. Han DKM, Haudenschild CC, Hong MK, Tinkle BT, Leon MB, Liau G. Evidence for apoptosis in human atherogenesis and in a rat vascular injury model. *Am J Pathol.* 1995;147:267–277.
30. Cho A, Courtman DW, Langille BL. Apoptosis (programmed cell death) in arteries of the neonatal lamb. *Circ Res.* 1995;76:168–175.
31. Bochaton-Piallat ML, Gabbiani F, Redard M, Desmouliere A, Gabbiani G. Apoptosis participates in cellularity regulation during rat aortic intimal thickening. *Am J Pathol.* 1995;146:1059–1064.
32. Bennett MR, Macdonald K, Chan SW, Boyle JJ, Weissberg PL. Cooperative interactions between RB and p53 regulate cell proliferation, cell senescence, and apoptosis in human vascular smooth muscle cells from atherosclerotic plaques. *Circ Res.* 1998;82:704–712.
33. Morgenbesser SD, Williams BO, Jacks T, DePinho RA. p53-dependent apoptosis produced by Rb-deficiency in the developing mouse lens. *Nature.* 1991;371:72–74.
34. Qin XQ, Livingston DM, Kaelin WG, Adams PD. Deregulated transcriptional factor E2F-1 expression leads to S-phase entry and p53-mediated apoptosis. *Proc Natl Acad Sci U S A.* 1994;91:10918–10922.
35. Miyashita T, Harigai M, Hanada M, Reed JC. Identification of a p53-dependent negative response element in the bcl-2 gene. *Cancer Res.* 1994;54:3131–3135.
36. Miyashita T, Reed JC. Tumor suppressor p53 is a direct transcriptional activator of the human bax gene. *Cell.* 1995;80:293–299.
37. Reed JC. Bcl-2 and the regulation of programmed cell death. *J Cell Biol.* 1994;124:1–6.
38. Bennett MR, Evan GI, Schwartz SM. Apoptosis of rat vascular smooth muscle cells is regulated by p53-dependent and -independent pathways. *Circ Res.* 1995;77:266–273.
39. Johnson TM, Epstein SE, Finkel T. Species-specific induction of apoptosis in normal vascular smooth muscle cells using an adenoviral expressing human p53. *Circulation.* 1996;94:I-155. Abstract.

Proc. Natl. Acad. Sci. USA
Vol. 95, pp. 3408–3412, March 1998
Biochemistry

EXHIBIT C

Crystal structure of the catalytic domain of human tumor necrosis factor-α-converting enzyme

KLAUS MASKOS*†, CARLOS FERNANDEZ-CATALAN*†, ROBERT HUBER*, GLEB P. BOURENKOV‡, HANS BARTUNIK‡, GEORGE A. ELLESTAD§, PRANITHA REDDY¶, MARTIN F. WOLFSON¶, CHARLES T. RAUCH¶, BEVERLY J. CASTNER¶, RAYMOND DAVIS¶, HOWARD R. G. CLARKE¶, MELISSA PETERSEN¶, JEFFREY N. FITZNER¶, DOUGLAS PAT CERRETTI¶, CARL J. MARCH¶, RAYMOND J. PAXTON¶, ROY A. BLACK¶, AND WOLFRAM BODE*‖

*Max-Planck-Institut für Biochemie, D-82152 Martinsried, Germany; ‡AG Proteindynamik MPG-ASMB c/o DESY, D-22603 Hamburg, Germany; §Wyeth–Ayerst Research, Pearl River, NY 10965; and ¶Immunex Corporation, Seattle, WA 98101

Contributed by Robert Huber, January 12, 1998

ABSTRACT **Tumor necrosis factor-α (TNFα) is a cytokine that induces protective inflammatory reactions and kills tumor cells but also causes severe damage when produced in excess, as in rheumatoid arthritis and septic shock. Soluble TNFα is released from its membrane-bound precursor by a membrane-anchored proteinase, recently identified as a multidomain metalloproteinase called TNFα-converting enzyme or TACE. We have cocrystallized the catalytic domain of TACE with a hydroxamic acid inhibitor and have solved its 2.0 Å crystal structure. This structure reveals a polypeptide fold and a catalytic zinc environment resembling that of the snake venom metalloproteinases, identifying TACE as a member of the adamalysin/ADAM family. However, a number of large insertion loops generate unique surface features. The pro-TNFα cleavage site fits to the active site of TACE but seems also to be determined by its position relative to the base of the compact trimeric TNFα cone. The active-site cleft of TACE shares properties with the matrix metalloproteinases but exhibits unique features such as a deep S3′ pocket merging with the S1′ specificity pocket below the surface. The structure thus opens a different approach toward the design of specific synthetic TACE inhibitors, which could act as effective therapeutic agents *in vivo* to modulate TNFα-induced pathophysiological effects, and might also help to control related shedding processes.**

Tumor necrosis factor-α (TNFα) (1), a major immunomodulatory and proinflammatory cytokine, is synthesized as a 223-aa membrane-anchored precursor. The soluble form of TNFα, comprising the C-terminal two-thirds of this precursor, is released into extracellular space by limited proteolysis at the Ala-76 → Val-77 bond. The proteinase responsible for this cleavage, called TACE or ADAM 17, has recently been identified (2, 3) as a zinc-endopeptidase consisting of a multidomain extracellular part, an apparent transmembrane helix and an intracellular C-terminal tail. The extracellular part comprises an N-terminal pro domain, a 259-residue catalytic domain, and a Cys-rich moiety that has been hypothesized to be composed of a disintegrin-like, an epidermal growth factor-like, and a crambin-like domain (2). Its polypeptide sequence, in particular, that accounting for the catalytic domain, indicates some similarity with other metzincins (4, 5), especially with the adamalysins/ADAMs (6–8) (a protein family comprising snake venom metalloproteinases and membrane-anchored surface proteins containing an adamalysin-like catalytic domain) and the matrix metalloproteinases (MMPs). In comparison to enzymes in these families, however, the polypeptide chain of the TACE catalytic domain is clearly longer and is stable in the absence of calcium. Further, in contrast to the MMPs, TACE is relatively insensitive to the tissue inhibitor of metalloproteinases-1 (TIMP-1) (9) and exhibits a different inhibition pattern toward synthetic inhibitors (9–12). In contrast to the MMPs, TACE cleaves a 12-mer peptide spanning the cleavage site in pro-TNFα selectively between Ala and Val (9). TNFα has been implicated in various deleterious physiological conditions such as rheumatoid arthritis, cachexia, and endotoxic shock; thus, blocking its release into the circulation by inhibitors might provide major therapeutic benefits (10–13).

We have undertaken an x-ray crystal structure analysis of the catalytic domain of TACE. This experimental model clarifies the structural and evolutionary relationships of TACE to other metzincins and will allow the structure-based design of TACE inhibitors capable of discriminating against other structurally related enzymes.

MATERIALS AND METHODS

A DNA construct encoding the pro and the catalytic domain of human TACE (residues 1–477), with Ser-266 changed to Ala and Asn-452 to Gln to prevent N-linked glycosylation, and with the sequence Gly-Ser-$(His)_6$ added to the C terminus to facilitate purification, was expressed in CHO cells (R.A.B., unpublished data). These cells primarily secreted processed TACE, about half of which began with Val-212 and half with Arg-215. This mature proteinase mixture was purified by NTA-Ni affinity chromatography followed by gel filtration, and was cocrystallized with the Immunex compound 3, *N*-{D,L-[2-(hydroxyamino-carbonyl)methyl]-4-methylpentanoyl}L-3-(tert-butyl)glycyl-L-alanine at room temperature in about 20% isopropanol, 20% PEG4000, and 0.1 M citrate, pH 5.4, by using the sitting drop vapor diffusion technique. These crystals belong to the monoclinic space group $P\,2_1$, have cell constants a = 61.38 Å, b = 126.27 Å, c = 81.27 Å, β = 107.41°, and contain four molecules in the asymmetric unit.

Anomalous diffraction data to 2.0 Å were collected with a MAR345 imaging plate scanner at 100 K on the BW6 wiggler beam line of DORIS (Deutsches Elektronen Synchrotron, Hamburg, Germany), by using monochromatic x-ray radiation at the wavelengths of maximal f″ (1.2769 Å) and minimal f′

Abbreviations: TNFα, tumor necrosis factor-α; TACE, TNFα converting enzyme; ADAM, a disintegrin and metalloprotease; MMP, matrix metalloproteinase; TIMP, tissue inhibitor of metalloproteinase.

Data deposition: The atomic coordinates and structure factors have been deposited at the Protein Data Bank, Biology Department, Brookhaven National Laboratory, Upton, NY 11973 (accession no. BNL-21333).

†K.M. and C.F.-C. contributed equally to this work.

‖To whom reprint requests should be addressed. e-mail: bode@biochem.mpg.de.

The publication costs of this article were defrayed in part by page charge payment. This article must therefore be hereby marked "*advertisement*" in accordance with 18 U.S.C. §1734 solely to indicate this fact.

(1.2776 Å) at the K absorption edge of zinc and at a remote wavelength (1.060 Å). These data were evaluated and scanned by using DENZO/SCALEPACK (14), yielding 77,653 independent reflections from 1,051,836 measurements (96.9% completeness, *R*-merge 0.031 in intensities).

All attempts to solve the crystal structure by Patterson search/molecular replacement methods by using modified adamalysin models failed to give useful starting positions for phasing. Thus, the four independent zinc atoms were located from an anomalous difference Patterson synthesis. Multiple wavelength anomalous diffraction phases were refined (yielding 5.0 and −5.1 electrons for f″ and f′ at 1.2769 Å, and 2.6 and −9.0 electrons for f″ and f′ at 1.2776 Å) and calculated with MLPHARE (15) including all measured data to 2.0 Å resolution. Their initial mean-figure-of-merit of 0.53 was increased to 0.76 by solvent flattening/histogram matching methods applying the program DM (16). This density allowed building of the complete chains of the four independent TACE catalytic domains and the bound hydroxamic acid inhibitors on an SGI graphic station by using TURBO-FRODO (17). This model was crystallographically refined with XPLOR (18) and with REFMAC (19) without applying any noncrystallographic symmetry restraints.

Molecules 1 and 3 and 2 and 4 are defined from Asp-219 and Met-221, respectively, to Ser-474. The *R* factor of the model, comprising, besides the 4 protein molecules, 4 inhibitor molecules, 172 solvent molecules, and 4 zinc ions, is 18.6% (*R*-free, 27.4%) for 71,400 independent reflections from 12.0 to 2.0 Å resolution. The rms deviation from target bond values is 0.015 Å. Omitting 10 to 15 residues, the molecules show rms deviations of 0.22 (molecules 1 with 3, and 2 with 4) to 0.40 Å (the residual combinations), values close to the estimated experimental error. Considerable shifts are only visible in a few surface loops, in particular in the second "ear."

RESULTS AND DISCUSSION

The monoclinic crystals contain four molecules in the crystallographic asymmetric unit. The molecules are not arranged as separate symmetric tetramers, but form an infinite periodic structure without a transition. In spite of quite different crystal contacts, the four molecules have, except for shifts of a few surface loops, very similar structures allowing a common description of the essential structural features.

The TACE catalytic domain (Fig. 1) has the shape of an oblate ellipsoid, notched at its flat side to give a relatively small active-site cleft separating a small "lower" subdomain from an "upper" main molecular body (Fig. 2*b*). Central to it is a highly twisted, five-stranded β-pleated sheet (strands sI–sV, see Figs. 1 and 3) flanked on its convex side by α-helices hB and hB2 and on its concave side by helices hA and hC. β-strands sII and sIII are linked by a large "multiple-turn loop," a long "intermediate" α-helix (hB), and an adjacent short α-helix (hB2), all arranged on "top" of the β-sheet and thus fully shielding its central part from bulk water (Fig. 1). The multiple-turn loop is bulged out at two sites, giving rise to a "spur-like" and an "acidic" protuberance (visible in Fig. 2*b* on top of the molecule). The sIII–sIV linker terminates in a short "bulge" before entering the "edge" strand sIV, the only antiparallel β-strand. The sIV–sV connecting segment is dissected into two large "ear-like" surface loops, the first one nestling to the main molecular body (giving rise to the "blue" surface, center left in Fig. 2*b*), and a long β-hairpin loop (sIVa–sIVb) projecting from the molecular surface (upper left in Figs. 1 and 2*b*). A bulged-out loop links sV with the "active-site helix" hC, which is located in the center of the molecule and stops abruptly at the strictly conserved Gly-412. At this point, the chain kinks down to build the lower subdomain.

The C-terminal chain comprising the last 61 residues of the TACE catalytic domain (Fig. 3) first forms three short,

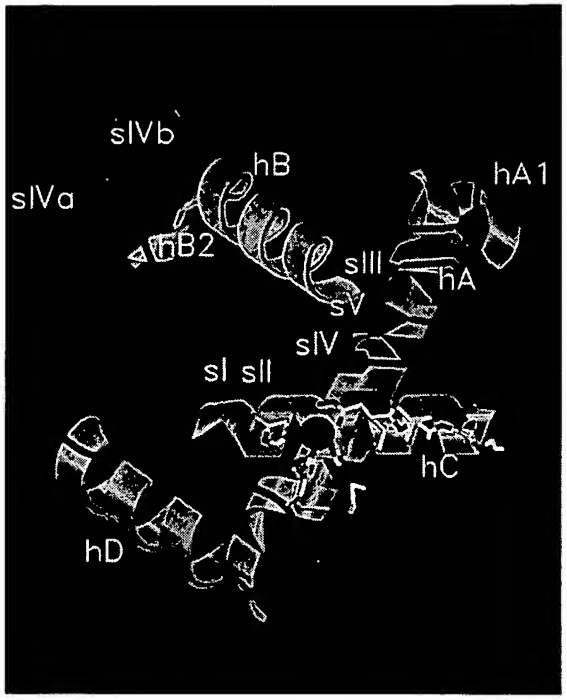

FIG. 1. Ribbon diagram of the TACE catalytic domain. The chain starts and ends on the lower and upper left backside, respectively. The three disulfides are shown as green connections and the catalytic zinc is shown as a pink sphere. His-405, His-409, His-415, Met-435, Pro-437, and the inhibitor (white) are shown with their full structure. The figure was made with SETOR (20).

straight, almost perpendicularly arranged segments linked by two "narrow," super-twisted loops. From there it returns via the tight "Met-turn" Tyr-433 → Val-434 → Met-435 → Tyr-436 back to the surface where it kinks at Pro-437 to form the Pro-437 → Ile-438 → Ala-439 outer "wall" of the S1′ crevice. Then, a wide loop precedes the C-terminal α-helix hD, after which the chain ends up on the molecular "back" surface close to the N terminus (Fig. 1). The first of the two "narrow" loops is disulfide-linked via Cys-423 → Cys-453 to the N terminus of helix hD. The C-terminal end of this helix is clamped to the "ear-like" sIV–sV linker peptide through Cys-365 → Cys-469. The spatially adjacent third disulfide bridge, Cys-225 → Cys-333, connects the N-terminal parts of β-strands sI and sIII. The last defined residues, Arg-473 and Ser-474, are fixed via hydrogen bonds to the main molecular body. In the intact TACE molecule, the following (presumably disintegrin-like) domain would probably pack to the "left back" surface side of the catalytic domain (see Fig. 5).

The active-site cleft of TACE (see Fig. 5) is relatively flat on the left-hand (nonprimed) side but becomes notched toward the right. The catalytic zinc residing in its center is pentacoordinated by the three imidazole Nε2 atoms of His-405, His-409, and His-415 (provided by the active-site helix and the following "descending" chain, together comprising the conserved zinc-binding consensus motif HEXXHXXGXXH) and by the carbonyl and the hydroxyl oxygens of the inhibitor's hydroxamic acid moiety, which presumably displaces a water molecule in the active enzyme (Figs. 4 and 5). This zinc-imidazole ensemble is placed above the distal ε-methyl-sulfur moiety of the strictly conserved Met-435, found in the Met-turn characteristic of the metzincin clan (5). Both carboxylate oxygens of the "catalytic" Glu-406 [which acts as a general base during catalysis (24)], squeezed between the zinc-liganding imidazole of His-405 and the edge strand, are hydrogen bonded to the hydroxyl and the N—H group of the hydroxamic acid (Fig. 4). Immediately to the right of the catalytic zinc invaginates the medium-sized, essentially hydrophobic, S1′

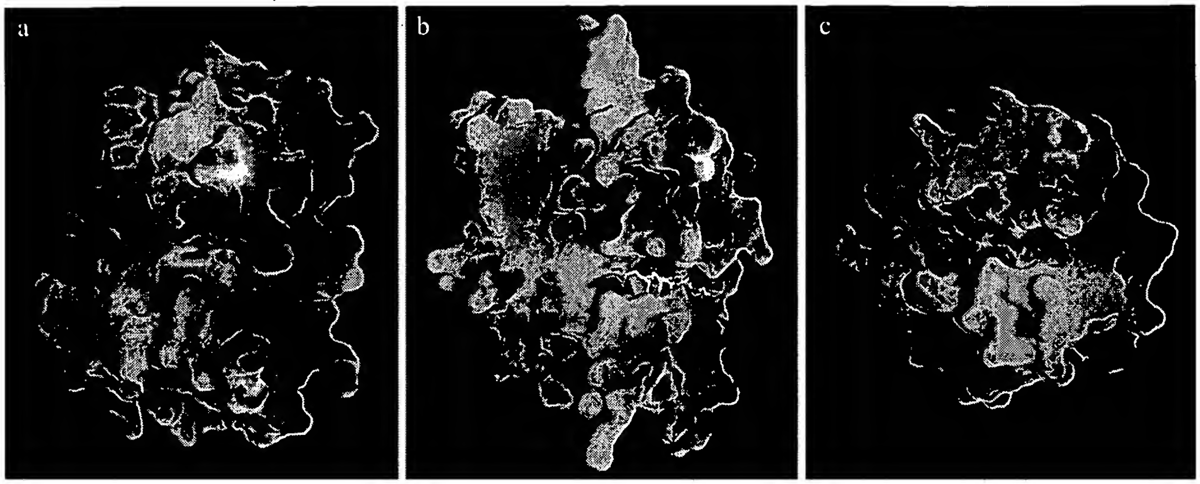

FIG. 2. Solid-surface representations of the catalytic domains of adamalysin II (6, 7) (*a*), TACE (*b*), and MMP-3 (*d*) (21). The electrostatic surface potentials are contoured from −20 (intense red) to 20 k_BT/e (intense blue). The active-site clefts run from left to right, with the catalytic zinc atoms (pink spheres) in the centers. In TACE, the bound inhibitor is shown in full structure. Orientations are equivalent to Fig. 1. The figure was made with GRASP (22).

specificity pocket (Figs. 2*b* and 5). Further to the right opens through a polar entrance a second hydrophobic (S3′) pocket, which merges inside the molecule with the S1′ pocket bridged by the opposing side chains of Ala-439 and Leu-348.

The (pseudo)peptidic part of the inhibitor binds in an extended geometry to the notched right-hand side of the active-site cleft, mimicking the interaction of the primed residues of a productively bound peptide substrate (Fig. 5). It runs antiparallel to the upper short bulge Gly-346 → Thr-347 → Leu-348 and parallel to the S1′ wall segment, forming two intermain-chain hydrogen bonds with each of them. The dominant intermolecular interactions are made by the P1′ isobutyl (pseudo-leucyl) side chain of the inhibitor and the hydrophobic bottleneck to the S1′ pocket, which accommodates three additional solvent molecules linked through a water channel to the adjacent S3′ pocket. The P2′ t-butyl side chain extends away from the enzyme, but nestles against the hydrophobic canopy formed by the enzyme's bulge. The P3′ Ala side chain points to the large S3′ pocket, but is too short to make favorable contacts. The C-terminal diaminoethyl group extends away from the cleft, adapting two different conformations in the four molecules.

The P1′ to P3′ segment Val-77 → Arg-78 → Ser-79 of a bound pro-TNFα will probably bind to TACE in a similar manner, with the isopropyl side chain of Val-77 just fitting into the hydrophobic S1′ neck, the Arg-78 side chain anchoring to the carbonyl and hydroxyl groups at the upper rim, and the Ser-79 hydroxyl interacting with the polar entrance to the S3′ pocket. The preceding P3 to P1 pro-TNFα residues Ala-74 → Gln-75 → Ala-76 most likely will align antiparallel to the edge strand, with their side chains extending into the S3 pocket and the (polar) shallow S2 depression, and projecting out of the

```
                                              sI        hA1
                                       →→→→→→|||||||||||
ADAM_CROAD       ..........  ......EQNL  PQRYIELVVV  ADRRVFMKYN
TACE         205 PEELVHR...  .VKRRADPDP  HKNTCKLLVV  ADHRFYRYMG 240
hADAM10          QEKHAINGPE  LLRKRRTTSA  EKNTCQLYIQ  TDHLFFKYYG

                           hA                         sII
                 ||||||||||||||||||||||||||||||       →→→→
ADAM_CROAD       .SDLNIIRTR  VHEIVNIINE  FYRSL.....  ...NIRVSLT
TACE         241 RGEESTTTNY  LIELIDRVDD  IYRNTSWDNA  GFKGYGIQIE 280
hADAM10          TRE..AVIAQ  ISSHVKAIDT  IYQTT..DFS  GIRNISFMVK

                  sII                                 hB
                 →→→                                ||||||||||
ADAM_CROAD       DLEIWSGQDF  I......TI.  ..........  QSSSSNTLNS
TACE         281 QIRILKSPQE  VKPGEKHYNM  AKSYPNEEKD  AWDVKMLLEQ 320
hADAM10          RIRINTTADE  KDPTNPF...  ..RFPN....  .ISVEKFLE.

                  hB   hB2               sIII         sIV
                 ||||| ||||||||       →→→→→        →→→
ADAM_CROAD       FGEWRERVLL  TRKRHDNAQL  LTAINFEGKI  IGKAYTS...
TACE         321 FSFDIAEEAS  ...KVCLAHL  FTYQDFDMGT  LGLAYVGSPR 357
hADAM10          ..LNSEQNHD  ...DYCLAYV  FTDRDFDDGV  LGLAWVGAP.

                            sIVa    sIVb      sV             hC
                             →→      →→     →→→→             ||||
ADAM_CROAD       .....SMCNP  ..........  .RSSVGIVKD  HSP....INL
TACE         358 ANSHGGVCPK  AYYSPVGKKN  IYLNSGLTST  KNYGKTILTK 397
hADAM10          SGSSGGICEK  SKLYSDGKKK  .SLNTGIITV  QNYGSHVPPK

                         hC
                 ||||||||||||||||||||
ADAM_CROAD       LVAVTMAHEL  GHNLGMEHDG  K....DCLRG  ........AS
TACE         398 EADLVTTHEL  GHNFGAEHDP  DGLAECAPNE  D......QGG 431
hADAM10          VSHITFAHEV  GHNFGSPHDS  G..TECTPGE  SKNLGQKENG

                                                 hD
                                      ||||||||||||||||||||||||
ADAM_CROAD       LCIMRPGLTP  GRS...YEFS  DDSMGYYQKF  LNQYKPQCIL
TACE         432 KYVMYPIAVS  GDHENNKMFS  NCSKQSIYKT  IESKAQECFQ 471
hADAM10          NYIMYARATS  GDKLNNNKFS  LCSIRNISQV  LEKKRNNCFV

ADAM_CROAD       NKP.......  ..........
TACE         472 ERSNKVCGNS  RVDEGEECDP 491
hADAM10          ESGQPICGNG  MVEQGEECDC
```

FIG. 3. Alignment of the catalytic domain sequences of adamalysin II (ADAM_CROAD) (7) and human ADAM 10 (hADAM10) (23) with TACE (2, 3). These sequences were aligned according to their topological equivalence and visually, respectively. Residue numbering is made according to the coded TACE sequence. Arrows and braces represent β-strands and α-helices in TACE. Blue symbols indicate topologically nonequivalent residues of adamalysin and TACE, and red designates residues that are identical in all three proteinases.

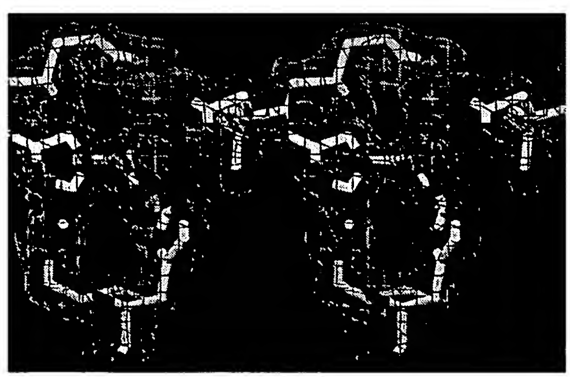

FIG. 4. Stereo section of the final 2.0 Å electron density around the catalytic zinc (pink sphere) superimposed with the final TACE model (with His-405 in the back, Glu-406 and the hydroxamic acid inhibitor moiety on top, His-409 to the left, and Met-435 and His-415 at the bottom). The average Zn—N or O distances are 2.3 Å. Orientation is similar to Fig. 1. Figure was made with TURBO-FRODO (17).

FIG. 5. Close-up view of the active-site cleft of TACE. On top of the solid surface representing the proteinase the bound inhibitor is shown in full structure, slotting with its isobutyl (P1′) and its Ala (P3′) side chains into the deep S1′ and the novel S3′ pockets. Figure was made as Fig. 2*b* (22).

(hydrophobic) cleft, respectively (Fig. 5). Thus, the preferential pro-TNFα cleavage at Ala-76 → Val-77 by TACE can partly be explained by favorable interactions in the active-site vicinity. Experimental evidence (25–27) suggests, however, that the cleavage site is also determined by its arrangement relative to the base of the compact cone (28) formed by the associated C-terminal segments of three pro-TNFα molecules (25). Preliminary docking experiments show, in fact, that the base of this TNFα-trimer cone [into which the six to eight disordered N-terminal TNFα residues ascend (28)] might be specifically recognized by the "right" side of the TACE catalytic domain, so that the pro-TNFα cleavage segment would precisely lock with its Ala-76 → Val-77 pair into the active site of TACE (Fig. 6). In addition, the processing of the membrane-bound pro-TNFα by TACE *in vivo* might be guided

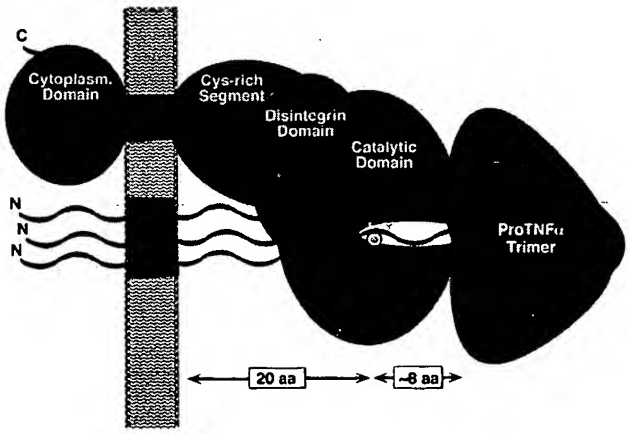

FIG. 6. Schematic model of the hypothetical pro-TNFα–TACE complex. The full-length activated TACE consists of the catalytic domain (shown in standard orientation, Fig. 1), a disintegrin-like domain, a Cys-rich moiety, the transmembrane segment, and the intracellular domain. The trimeric pro-TNFα consists of intracellular segments, transmembrane segments, 26–28 residue spacers forming a stalk, and the compact trimeric TNFα cone (28). TACE and pro-TNFα might be anchored in the membrane in such a manner that the TNFα cone is attached to the "right" side of the catalytic domain, with the scissile Ala-76 → Val-77 bond of one extended pro-TNFα strand placed above the active site.

by assembling, i.e., by the mode of presentation of the [presumably nonstructured (26)] pro-TNFα cleavage segment to the TACE active site at a defined distance from the anchoring membrane.

The polypeptide topology and in particular the surface presentation of the catalytic zinc reveal the catalytic domain of TACE to be a typical metzincin (4, 5), with closest similarities to the catalytic domain of snake venom metalloproteinases such as adamalysin II (6, 7, 29, 30) (Figs. 2*a* and 7). The close structural similarity is reflected by the superposition of the central β-sheet and the long α-helices and, in particularly, by a number of structural features that TACE shares exclusively with the adamalysins: the long helix hB and the preceding multiple-turn loop arranged on top of the β-sheet; the typically arranged and shaped C-terminal helix hD; and the extended C terminus placed on the backside surface. About 175 of the 259 TACE and 201 adamalysin residues are topologically equivalent (with a Cα-atom rms deviation of 1.3 Å), and 39 of them are identical (see Fig. 3). Additional structural features that confirm the close relationship of TACE to the adamalysins include: the loosely arranged N terminus; the characteristic Asp-416 (directly following the zinc-binding consensus motif, Fig. 3) involved in identical intramolecular hydrogen bond interactions; the adjacent disulfide bridge Cys-423 → Cys-453 linking the first narrow loop to the C-terminal helix hD [which TACE does not share with adamalysin II or atrolysin, but with the H2-proteinase from the snake venom of *Trimeresurus flavoviridis* (30)]; and disulfide bridge Cys-365 → Cys-469 connecting the sIV–sV linker with the C-terminal helix hD.

However, the catalytic domain of TACE also differs from adamalysin in several respects: with 259 residues, its chain is much longer; most of the additional residues of TACE are clustered, giving rise to the two surface protuberances of the multiple-turn loop, to the two "ears" of the sIV–sV linker, and to a more bulged-out sV-hC connector (see Figs. 3 and 7); TACE lacks an adamalysin-like calcium-binding site (though the disulfide bridge Cys-225 → Cys-333 in TACE serves the

FIG. 7. Superposition of the ribbons of the catalytic domain of TACE (gold) and adamalysin (blue) (6, 7). Also shown are the catalytic zinc of TACE (pink sphere) and the three (TACE) and two (adamalysin) disulfide bridges. Orientation is similar to Fig. 1. Figure was made with GRASP (22).

same function clamping the N-terminal chain to strand sIII); TACE has a deep S3′ pocket merging with its S1′ pocket; and the charge pattern in and around the primed subsites is inverted in TACE compared with adamalysin (Fig. 2 *a* and *b*).

This structure thus shows that TACE is not a typical member of the mammalian ADAMs but stands outside. TACE shares this role with ADAM 10, for which a TACE-like specificity has been demonstrated (23, 31) and whose *Drosophila* version (kuz) has recently been shown to process the transmembrane receptor Notch (32). ADAM 10, too, probably exhibits an elongated hA-sII loop and the two "ears" found in TACE, but might have a multiple-turn intermediate in size between TACE and adamalysin. Ninety-one of the ADAM 10 catalytic domain residues are identical to TACE (Fig. 3). The other mammalian ADAMs, in contrast, probably resemble adamalysin II much more closely (see ref. 7).

The structural homology between the catalytic domains of TACE and the MMPs is significantly lower. The relative arrangement of the common secondary structural elements differs more (reflected by the significantly larger rms deviation of 1.6 Å of the approximately 120 topologically equivalent Cα-atoms), and the MMPs lack characteristic TACE/adamalysin structural elements (such as the intermediate helix hB and the multiple-turn loop, the Asp residue following the third zinc-binding histidine) or exhibit common features (such as the structural zinc and the integrated calcium ions) not seen in TACE. Notwithstanding the obvious differences in secondary structure, the active-site cleft of TACE bears some similarity to that of the MMPs, with the flat, nonprimed (left-hand) side, and the narrow primed side centering around the S1′ pocket of varying size (Fig. 2 *b* and *c*). This subsite similarity to the MMPs explains the observed sensitivity of a TACE-like activity to synthetic hydroxamic acid inhibitors originally designed for inhibition of various MMPs (11). Model building experiments with the TIMP-1 structure (21) show no obvious steric interference in the active-site region that could explain why TACE is insensitive to the TIMPs (9); more detailed studies will hopefully allow the design of TIMP-variants with improved affinity for TACE in the near future.

This TACE crystal structure thus gives evidence for a substantial topological similarity between the catalytic domains of TACE and the adamalysins/ADAMs, and it shows that TACE's substrate-binding site resembles that of the MMPs. TACE exhibits, however, several structural peculiarities regarding surface charge and shape, which may enable the design of potent selective synthetic inhibitors. Such tailored inhibitors could be of wide use to study the physiological role of TACE, as well as that of TNFα, but, in particular, could also become valuable therapeutics of arthritic lesions and may increase the rate of survival in various endotoxin-induced septic shock syndromes (10). Such tailored inhibitors might clarify the role of TACE in the processing of other members of the TNF superfamily and in the shedding of a number of other cell surface proteins (12, 33).

We thank Mrs. M. Braun for excellent assistance with crystallization, J. Medrano for computing advice, R. Johnson, M. Gerhart, and M. DeJardin for protein analyses, and A. Woodward and B. Rasmussen for growing the CHO cells. The financial support by the SFB469, the Biotechnology Program (contract ERBBIO4-CT960464) of the European Union, the Bundesministerium für Bildung und Forschung, and the Fonds der Chemischen Industrie is kindly acknowledged.

1. Bemelmans, M. H. A., VanTits, L. J. H. & Buurman, W. A. (1996) *Crit. Rev. Immunol.* **16**, 1–11.
2. Black, R. A., Rauch, C. T., Kozlosky, C. J., Peschon, J. J., Slack, J. L., Wolfson, M. F., Castner, B. J., Stocking, K. L., Reddy, P., Srinivasan, S., *et al.* (1997) *Nature (London)* **385**, 729–733.
3. Moss, M. L., Jin, S. L. C., Milla, M. E., Burkhart, W., Carter, H. L., Chen, W. J., Clay, W. C., Didsberg, J. R., Hassler, D., Hoffman, C. R., *et al.* (1997) *Nature (London)* **385**, 733–736.
4. Bode, W., Gomis-Rüth, F.-X. & Stöcker, W. (1993) *FEBS Lett.* **331**, 134–140.
5. Stöcker, W., Grams, F., Baumann, U., Reinemer, P., Gomis-Rüth, F. X., McKay, D. B. & Bode, W. (1995) *Protein Sci.* **4**, 823–840.
6. Gomis-Rüth, F. X., Kress, L. F. & Bode, W. (1993) *EMBO J.* **12**, 4151–4157.
7. Gomis-Rüth, F. X., Kress, L. F., Kellermann, J., Mayr, I., Lee, X., Huber, R. & Bode, W. (1994) *J. Mol. Biol.* **239**, 513–544.
8. Wolfsberg, T. G. & White, J. M. (1996) *Dev. Biol.* **180**, 389–401.
9. Black, R. A., Durie, F. H., Otten-Evans, C., Miller, R., Slack, J. L., Lynch, D. H., Castner, B., Mohler, K. M., Gerhart, M., Johnson, R. S., *et al.* (1996) *Biochem. Biophys. Res. Commun.* **225**, 400–405.
10. Mohler, K. M., Sleath, P. R., Fitzner, J. N., Cerretti, D. P., Alderson, M., Kerwar, S. S., Torrance, D. S., Otten-Evans, C., Greenstreet, T., Weerawarna, K., *et al.* (1994) *Nature (London)* **370**, 218–220.
11. DiMartino, M., Wolff, C., High, W., Stroup, G., Hoffman, S., Laydon, J., Lee, J. C., Bertolini, D., Galloway, W. A., Crimmin, M. J., *et al.* (1997) *Inflamm. Res.* **46**, 211–215.
12. Crowe, P. D., Walter, B. N., Mohler, K. M., Otten-Evans, C., Black, R. A. & Ware, C. F. (1995) *J. Exp. Med.* **181**, 1205–1210.
13. Moreland, L. W., Baumgartner, S. W., Schiff, M. H., Tindall, E. A., Fleischmann, R. M., Weaver, A. L., Ettlinger, R. E., Cohen, S., Koopman, W. J., Mohler, K., *et al.* (1997) *N. Engl. J. Med.* **337**, 141–147.
14. Otwinowski, Z. & Minor, W. (1993) *DENZO: A Film Processing for Macromolecular Crystallography* (Yale University, New Haven, CT).
15. Otwinowski, Z. (1991) in *Isomorphous Replacement and Anomalous Scattering, Daresbury Study Weekend Proceedings* (SERC Daresbury Laboratory, Warrington, U.K.).
16. Cowtan, K. (1994) *Joint CCP 4 ESF-EACBM Newsletter on Protein Crystallography* **31**.
17. Roussel, A. & Cambilleau, C. (1989) *turbo-frodo in Silicon Graphics Geometry*, Partners Directory (Silicon Graphics, Mountain View, CA).
18. Brünger, A. T. (1991) *Curr. Opin. Struct. Biol.* **1**, 1016–1022.
19. Collaborative Computational Project Number 4. (1994) *Acta Crystallogr.* **D50**, 760–763.
20. Evans, S. V. (1993) *J. Mol. Graph.* **11**, 134–138.
21. Gomis-Rüth, F. X., Maskos, K., Betz, M., Bergner, A., Huber, R., Suzuki, K., Yoshida, N., Nagase, H., Brew, K., Bourenkov, G. P., *et al.* (1997) *Nature (London)* **389**, 77–81.
22. Nicholls, A., Bharadwaj, R. & Honig, B. (1993) *Biophys. J.* **64**, A166.
23. Rosendahl, M. S., Ko, S. C., Long, D. L., Brewer, M. T., Rosenzweig, B., Hedl, E., Anderson, L., Pyle, S. M., Moreland, J., Meyers, M. A., *et al.* (1997) *J. Biol. Chem.* **272**, 24558–24593.
24. Grams, F., Reinemer, P., Powers, J. C., Kleine, T., Pieper, M., Tschesche, H., Huber, R. & Bode, W. (1995) *Eur. J. Biochem.* **228**, 830–841.
25. Tang, P., Hung, M.-C. & Klostergaard, J. (1996) *Biochemistry* **35**, 8216–8225.
26. Tang, P., Hung, M.-C. & Klostergaard, J. (1996) *Biochemistry* **35**, 8226–8233.
27. Perez, C., Albert, I., DeFay, K., Zachariades, N., Gooding, L. & Kriegler, M. (1990) *Cell* **63**, 251–258.
28. Jones, E. Y., Stuart, D. I. & Walker, N. P. C. B. (1989) *Nature (London)* **338**, 225–228.
29. Zhang, D., Botos, I., Gomis-Rüth, F. X., Doll, R., Blood, C., Njoroge, F. G., Fox, J. W., Bode, W. & Meyer, E. F. (1994) *Proc. Natl. Acad. Sci. USA* **91**, 8447–8451.
30. Kumasaka, T., Yamamoto, M., Moriyama, H., Tanaka, N., Sato, M., Katsube, Y., Yamakawa, Y., Omori-Satoh, T., Iwanaga, S. & Ueki, T. (1996) *J. Biochem.* **119**, 49–57.
31. Lunn, C. A., Fan, X., Dalie, B., Miller, K., Zavodny, P. J., Narula, S. W. & Lundell, D. (1997) *FEBS Lett.* **400**, 333–335.
32. Pan, D. & Rubin, G. M. (1997) *Cell* **90**, 271–280.
33. Hooper, N. M., Karran, E. H. & Turner, A. J. (1997) *Biochem. J.* **321**, 265–279.